Lithos 192–195 (2014) 240–258

Contents lists available at ScienceDirect

Lithos

journal homepage: www.elsevier.com/locate/lithos

Miocene magmatic evolution in the Nefza district (Northern Tunisia) and its relationship with the genesis of polymetallic mineralizations

Sophie Decrée [a,b,*], Christian Marignac [c], Jean-Paul Liégeois [b], Johan Yans [d], Randa Ben Abdallah [e], Daniel Demaiffe [f]

[a] Institut Royal des Sciences Naturelles de Belgique — Service Géologique de Belgique, 29 Rue Vautier, B-1000 Bruxelles, Belgique
[b] Musée Royal de l'Afrique Centrale, Geodynamics and Mineral Resources, 13 Leuvensesteenweg, B-3080 Tervuren, Belgique
[c] Géologie et Gestion des Ressources Minérales et Energétiques — G2R (CNRS/Université Henri Poincaré), Ecole Nationale Supérieure des Mines de Nancy, Campus ARTEM, F-54042 Nancy, France
[d] Université de Namur, Département de Géologie, 61 rue de Bruxelles, B-5000 Namur, Belgique
[e] Laboratoire de Valorisation des Matériaux Utiles-CNRSM Technopôle de Borj Cédria BP 273, 8020 Soliman-Tunisie, Tunisia
[f] Université Libre de Bruxelles (ULB), CP 160/02, Laboratoire de géochimie - DSTE, 50 av. F. Roosevelt, B-1050 Bruxelles, Belgique

ARTICLE INFO

Article history:
Received 26 March 2013
Accepted 1 February 2014
Available online 15 February 2014

Keywords:
Cenozoic magmatism
Polymetallic mineralizations
Post-collisional
Sr–Nd–Pb isotopes
Nefza
Tunisia

ABSTRACT

The Nefza mining district in Northern Tunisia comprises late Miocene (Serravallian to Messinian) magmatic rocks belonging to the post-collisional magmatism of the Mediterranean Maghreb margin. They are mainly made up of Serravallian granodiorite (Oued Belif massif), Tortonian rhyodacites (Oued Belif and Haddada massifs) and cordierite-bearing rhyodacites (Ain Deflaia massif) in addition to rare Messinian basalts. They are all characterized by LILE and LREE enrichment and strong enrichment in Pb and W. The Messinian basalts, which are also enriched in LILE, exhibit transitional characteristics between calc-alkaline and alkaline basalts.

Geochemical (major and trace elements) and Sr, Nd and Pb isotopic compositions indicate that: (1) granodiorite is linked to the differentiation of a metaluminous calc-alkaline magma derived from a lithospheric enriched mantle source and contaminated by old crustal materials; (2) rhyodacites result from the mixing of the same metaluminous calc-alkaline magma with variable proportions of melted continental crust. Cordierite-bearing rhyodacite, characterized by the highest $^{87}Sr/^{86}Sr$ isotopic ratios, is the magma comprising the highest crustal contribution in the metaluminous–peraluminous mixing and is close to the old crustal end-member; (3) late basalts, transitional between the calc-alkaline and alkaline series, originated from an enriched mantle source at the lithosphere–asthenosphere boundary.

In the Nefza mining district, magmatic rock emplacement has enhanced hydrothermal fluid circulation, leading to the deposition of polymetallic mineralizations (belonging to the Iron–Oxide–Copper–Gold and the sedimentary exhalative class of deposits, among others). Magmatic rocks are also a source for the formation of lead (and probably other metals) in these deposits, as suggested by their Pb isotopic compositions.

Magmatic rock emplacement and connected mineralization events can be related to the Late Mio-Pliocene reactivation of shear zones and associated lineaments inherited from the Variscan orogeny.

1. Introduction

The Nefza mining district of Northern Tunisia (Fig. 1), although extending over a rather small area, displays a wide variety of Middle–Late Miocene magmatic rocks, from plutonic granodiorite to (sub-)volcanic rhyodacite and basalt, related to the Cenozoic circum-Mediterranean geodynamic history. The Nefza magmatism is especially related to the development of the Maghreb indenter that acted as a locking zone during the regional compression phase, inducing lithospheric breaks, which favored the partial melting of the consequently rising asthenosphere. These events started in Central Eastern Algeria during the Langhian age (16–14 Ma; lower Miocene) and propagated both eastwards and westwards (Maury et al., 2000; Piqué et al., 1998). In the Nefza district, the post-collisional calc-alkaline rocks (granodiorite and rhyodacite) emplaced during the Serravallian–Tortonian age and the basalts during the Messinian age.

* Corresponding author at: Institut Royal des Sciences Naturelles de Belgique — Service Géologique de Belgique, 29 Rue Vautier, B-1000 Bruxelles, Belgique.
E-mail addresses: sophie.decree@naturalsciences.be (S. Decrée), christian.marignac@mines.inpl-nancy.fr (C. Marignac), jean-paul.liegeois@africamuseum.be (J.-P. Liégeois), johan.yans@fundp.ac.be (J. Yans), randa.benabdallah@gmail.com (R. Ben Abdallah), ddemaif@ulb.ac.be (D. Demaiffe).

http://dx.doi.org/10.1016/j.lithos.2014.02.001
0024-4937/

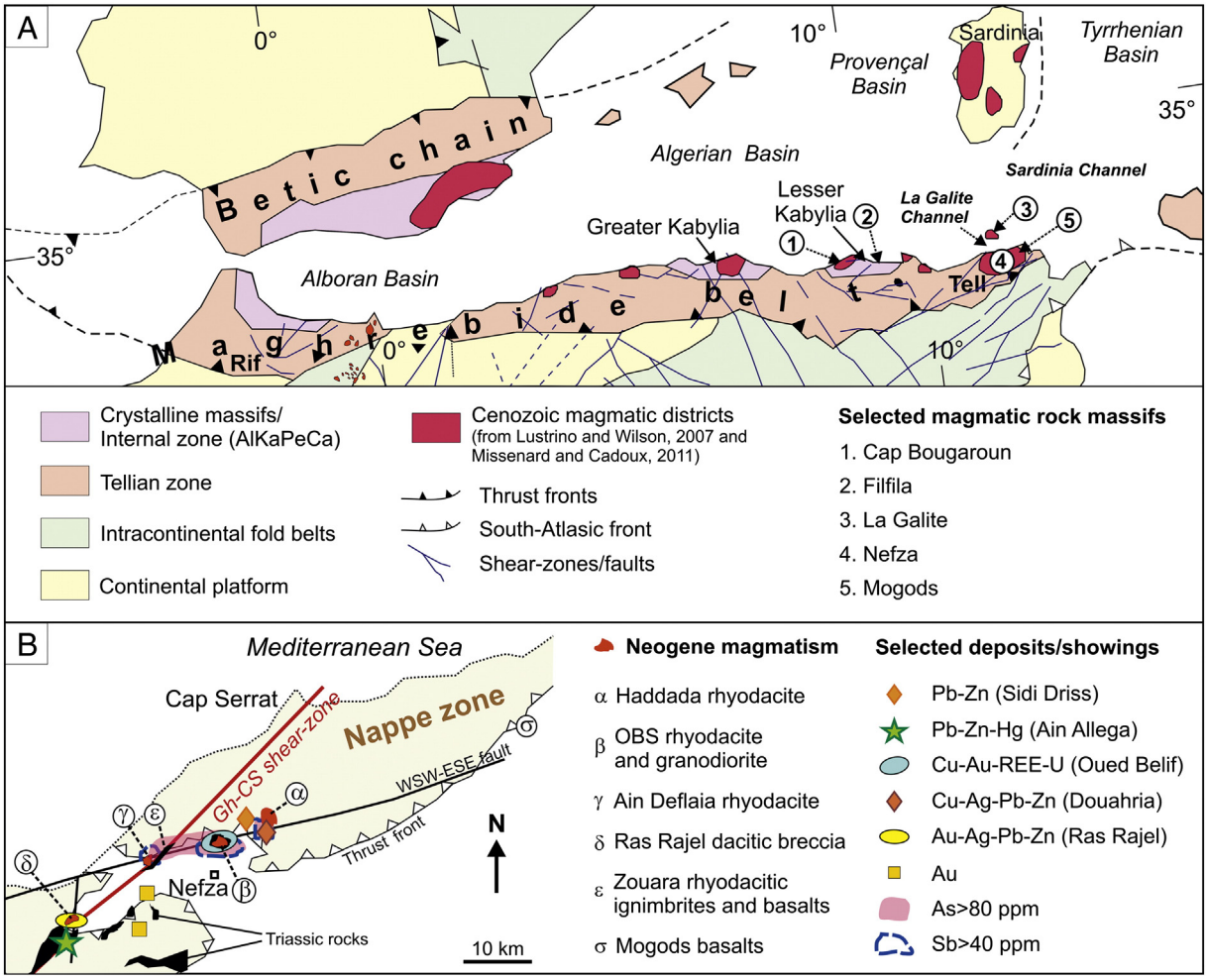

Fig. 1. A. Tectonic sketch map of the western Mediterranean region (modified after Piqué et al., 1998; Bouaziz et al., 2002), with Cenozoic magmatic districts (from Lustrino and Wilson, 2007 and Missenard and Cadoux, 2012); B. Structural settings and mineralizations in the Tunisian Nappe Zone (modified from Gharbi, 1977 and Albidon Limited, 2004; As and Sb anomalies are personal communications from the Office National des Mines de Tunisie) (modified from Decrée et al., 2013); Gh-CS is for the Ghardimaou-Cap Serrat shear-zone.

According to Maury et al. (2000), the Nefza calc-alkaline rocks (granodiorite and rhyodacite) resulted from the partial melting of the lithospheric mantle, previously metasomatised during the Eocene by oceanic subduction caused by the uprise of the asthenosphere. Available isotopic data indicate a significant contamination of the mantle-derived magma(s) by a heterogeneous continental crust (Maury et al., 2000). The younger Messinian basalts of the Nefza and Mogods (~40 km to the NE of Nefza) areas display mineralogical and chemical features which are transitional between calc-alkaline and alkali basalts (Halloul and Gourgaud, 2012). They result from partial melting of the mantle generated in the uprising lithosphere–asthenosphere boundary during the widening of the lithospheric break (Maury et al., 2000).

The petrographical and geochemical characteristics (major and trace elements) of the Nefza magmatic rocks have been regularly studied (Badgasarian et al., 1972; Bellon, 1976; Faul and Foland, 1980; Halloul, 1989; Halloul and Gourgaud, 2012; Laridhi Ouazaa, 1989a,b, 1990; Mauduit, 1978; Metrich-Travers, 1976; Tzekova, 1975) but no detailed isotopic studies have been performed on these rocks to this day. The aim of this study is to reconsider the magmatic processes leading to the formation of the various Nefza district magmatic rocks on the basis of literature data, new geochemical (major and trace elements) and isotopic data (Pb, Sr, Nd). In addition, the Pb isotopic data obtained on regional polymetallic mineralization (Pb–Zn–Fe–REE–U–Au–Cu–Hg; e.g. Abidi et al., 2010, 2011, 2012; Decrée et al., 2008a,b, 2010, 2013) allow us to reconsider magmatic contribution as a heat and metal source to the mineralization process.

2. Geological context

2.1. The Maghrebide belt

The Maghrebide belt, running E–W in Northern Africa, belongs to the Western Mediterranean Alpine belt stretching west to east from the Betic Cordillera in Spain to the Apennine Belt in Italy (Fig. 1A). It resulted from the collision between the African plate (part of the former Gondwana supercontinent) and a microplate called "Meso-Mediterranean" derived from the European continent during the Neo-Tethysian oceanic aperture in the Early Jurassic. The collision was followed by the eastward migration of the former subduction front and the opening of back-arc basins, namely the present-day oceanic West Mediterranean basin (Gueguen et al., 1998; Jolivet, 2008, and references therein). The Meso-Mediterranean microplate, now preserved as "internal crystalline massifs" within the Maghrebide and Betic belts, is also known as "Alkapeca", an acronym formed from the initial letters of the Alboran basin (which has a thin continental crust) and the names of the main internal massifs stretching from west to east: the Kabylian massifs in Algeria and the Peloritain mountains in Sicily and Calabria (Bouillin, 1977; Guerrera et al., 1993) (Fig. 1A).

The present-day Maghrebide belt consists of three areas stretching from north to south: (i) the Internal Zone, comprising the internal massifs and a Flysch Zone, which is overthrust towards (ii) the Tellian Zone (or Tellian Atlas), which is in turn overthrust towards (iii) a deformed foreland (Saharan platform and intracontinental Atlas fold belts, the

latter corresponding to inverted extensional basins). The main thrust limiting the Tellian Zone to the south runs along the northern coast of Africa towards northeastern Tunisia and northward to Sicily (Fig. 1A). This structure was generated according to three main steps (Frizon de Lamotte et al., 2000, 2006, and references therein): (1) in the late Cretaceous period, the subduction of the Tethyan oceanic strip, which separated Gondwana from Alkapeca resulted in a flysch accretion prism ("Kabylian flyschs") in the Eastern Maghrebides; (2) docking of the Alkapeca domain (Middle Eocene–Early Oligocene) with the Africa margin, altogether deformed (Bouillin, 1977); (3) the Alpine phase s.s. (Latest Burdigalian–Early Serravallian) resulted from the collision between the dismembered Alkapeca and Africa domains, generating the large thrusts described above. During Neogene, when the studied Nefza magmatism emplaced, there was an alternation of oblique compressive regime and extension regime, which is typical of the post-collisional period (Liégeois et al., 1998). Most important, during the Serravallian and the Tortonian periods, the northern African realm was affected by a very oblique compressive regime, with "out of sequence" thrusts in the Atlasic domain (Benaouali-Mebarek et al., 2006), and experienced short-lived returns to extensional conditions during the Messinian and Pliocene periods. Since then, the Africa–Europe convergence rate has been very low (0.5 $cm.a^{-1}$) and the plate boundary is still located at the front of the Tellian Zone (Jolivet, 2008), with some folding just to the north of the coastline (Yelles-Chaouche et al., 2006).

In the Eastern Maghrebides, felsic magmatism post-dated the thrusting and propagated eastward from the more internal zones toward the external zones (Maury et al., 2000; and references therein). In the internal zones, granite/granodioritic plutonism and dacite/rhyolite subvolcanic intrusions occurred (1) during the later Burdigalian and Langhian periods in the Kabylian and Edough massifs of Eastern Algeria, (2) during the Serravallian in the Galite Island of Northern Tunisia and (3) during the Serravallian and Tortonian in the flysch zone of Northern Tunisia.

The source of this potassic calc-alkaline post-collisional magmatism is the subcontinental lithospheric mantle (SCLM) metasomatized during an earlier subduction event (early Alpine or Variscan in age) mixed with partial melts generated within the African crust (Maury et al., 2000). The melting of this composite source may be ascribed to the rise of the asthenospheric mantle as a result of lithospheric delamination (Maury et al., 2000), possibly triggered by the Miocene reactivation of lithospheric-scale shear-zones inherited from the Variscan orogeny (Piqué et al., 1998, 2002). In Northern Tunisia, this felsic magmatism event was followed by minor amounts of Messinian basalts.

2.2. The Nefza district

In the Nefza district, studied here, the sedimentary substrate comprises the Ed Diss thrust sheet (Upper Cretaceous to Eocene) overlain by the Numidian nappe (Rouvier, 1977) (Fig. 2). The latter consists of a thick (≥1000 m) series of siliciclastic flysch (Numidian flysch), Oligocene to Lower Miocene (Burdigalian) in age (c 34–16 Ma).

The whole nappe pile is crosscut by Upper Miocene felsic plugs and mafic dikes (Jallouli et al., 2003 and references therein). *The Jebel Haddada massif*, located at the eastern end of the district (Fig. 2), comprises a rhyodacitic dome and cinerites (preserved, even though altered, in the Douahria Fe-rich sediments). This rhyodacitic dome is dated between 8.7 ± 0.15 Ma and 8.2 ± 0.4 Ma (K–Ar biotite ages and Rb–Sr whole rock ages; Table 1; Bellon, 1976; Faul and Foland, 1980). To the west of the Jebel Haddada massif, *the Oued Belif elliptic structure* (Fig. 2) encloses two generations of middle to late Miocene subvolcanic rocks: the Ragoubet el-Alia granodiorite (12.9 ± 0.5 Ma, Serravallian; Bellon, 1976) and the Ragoubet Es-Seid and Oued Arrar rhyodacites (8.3 ± 0.8 and 8.9 ± 0.15 Ma, Tortonian; Badgasarian et al., 1972; Faul and Foland, 1980). *The Ain Deflaia dome*, to the west, is made up of felsic magmatic rocks (Fig. 2); it comprises a cordierite-bearing rhyodacite dated at 12.3 ± 0.5 Ma and 8.5 Ma (whole-rock Rb–Sr and biotite K–Ar; Bellon, 1976; Rouvier, 1977). Pyroclastic deposits (perlitic rhyolites and rhyodacites; Laridhi Ouazaa, 1988, 1989b) partly fill the Zouara basin. Laridhi Ouazaa (1988, 1989b, 1996) emphasized the geochemical and mineralogical similarities between the Ain Deflaia massif and the Zouara pyroclastites. Transitional basalt sills outcrop at Mokta el-Hadid in the *Zouara basin* (Fig. 2); they have been dated at 8.4 ± 0.4 Ma by Bellon (1976) and at 6.9 ± 0.3 Ma and 6.4 ± 0.15 Ma by Rouvier (1977).

Geophysical work (Jallouli et al., 2003) led to the recognition of a very shallow concealed magmatic sill (0.5 to 1.5 km depth, 0.7 to 0.9 km thick, diameter of c. 20 km) under the whole area under study. This sill can be regarded as the root of the Oued Belif intrusions (Jallouli et al., 2003) and is thought to have been intruded (like the granodiorite) during the Alpine compression phase, from Upper Langhian to Serravallian (Bouaziz et al., 2002). The later Tortonian–Messinian basalts were emplaced during the extensional phase (Jallouli et al., 2003; Mauduit, 1978; Maury et al., 2000) that began during that period (Bouaziz et al., 2002). In the Nefza district, the Mokta el-Hadid basalts and the Ras Rajel dacitic breccias emplaced along the NE–SW Guardimaou-Cap Serrat sinistral major shear-zone.

2.3. Neighbouring areas

In the Northern Tunisian Tell region (Fig. 1A), magma emplacements are related to lithospheric breaks induced by the Maghreb indenter (Maury et al., 2000; Piqué et al., 1998). This model is supported by the presence of a thinner lower crust (10 km in the Tell region vs. 20 km in Central Tunisia; Jallouli and Mickus, 2000) and by the reactivation of NE–SW and NW–SE basement shear-zones inherited from the Variscan orogeny (Piqué et al., 2002).

In the Mogods area, alkaline basalts (Mauduit, 1978; Maury et al., 2000; Figs. 1 and 2) were emplaced, as in the Nefza district, along NE–SW and NW–SE shear-zones between 7 ± 1 Ma and 5.17 ± 0.04 Ma (Bellon, 1976; Rouvier, 1977; Talbi et al., 2005).

2.4. The Nefza polymetallic mineralizations

In the Nefza district, one of these NE–SW and NW–SE shear-zones, the Guardimaou-Cap Serrat sinistral major shear-zone, in addition to Late Miocene extrusions, is punctuated by a series of local mineral showings and deposits: mercury mineralization at Ain Allega, Pb–Zn MVT deposits (Abidi et al., 2010, 2012; Gharbi, 1977) and Ag–Au showings at Ras Rajel (the dacitic breccias contain up to 48 g/t Ag, 0.3% Zn, 0.5% Pb and 52 ppb Au; Albidon Limited, 2004). The Nefza felsic magmatism was emplaced along a second set of slightly oblique – WSW to ESE oriented – fractures. Similarly, the Oued Belif structure and associated IOCG mineralization (Decrée et al., 2013), the Messinian Zn–Pb sedex deposits of Sidi Driss and Douahria (Decrée et al., 2008a), the post-Messinian lateritic ore (Decrée et al., 2008b, 2010) and even regional As and Sb geochemical anomalies (Office National des Mines de Tunisie, oral comm) (Fig. 1B) are located along such fractures.

Among these deposits, the Oued Belif breccia, enclosing the Ain El-Alia granodiorite, the Ragoubet Es-Seid and the Oued Arrar rhyodacites, is marked by Fe–REE–U mineralization belonging to the IOCG class of deposits (Decrée et al., 2013). This mineralization and its associated alterations are related to very high-temperature fluid circulations (≥500–550 °C; Talbi et al., 1999), for which only a close magma chamber can supply the necessary heat. Moreover, the Oued Belif geochemical fingerprint suggests a contribution from the felsic and mafic magmatism, either as a direct magmatic-hydrothermal contribution or through brine leaching. This is sustained by the presence of a volcanic ash component within the breccia suggesting that brecciation could be related to a phreato-magmatic event (Decrée et al., 2013; Mauduit, 1978; Perthuisot, 1978).

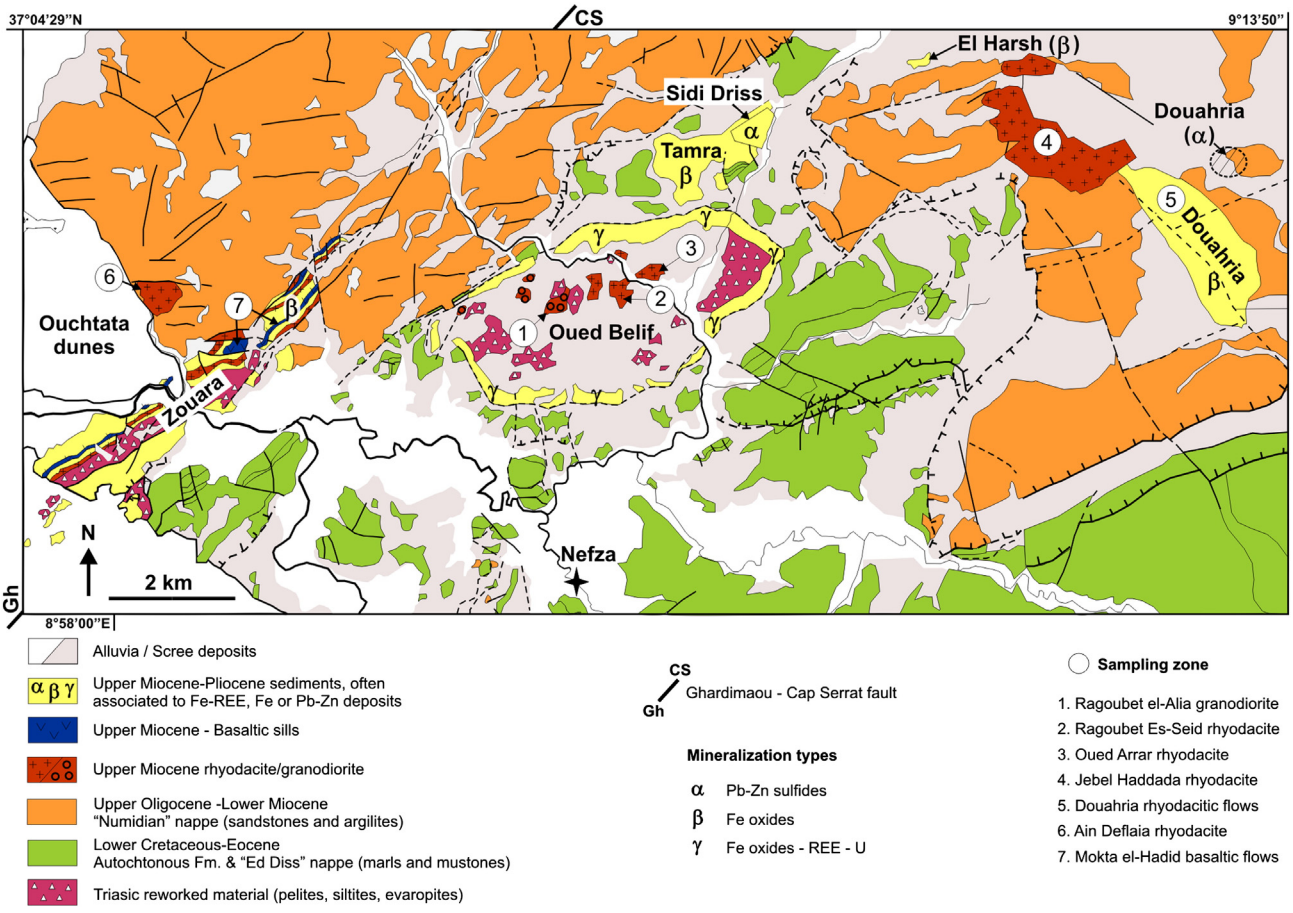

Fig. 2. Geological sketch map of the studied area (modified and redrawn from Gottis and Sainfeld, 1952; Batik, 1980 and Rouvier, 1987), with location of selected showings/deposits and magmatic rock sampling zones.

In the Nefza area, the Messinian sedex Pb–Zn deposits of Sidi Driss and Douahria are also related to thermally driven fluid circulation linked either to Messinian mafic magmatism and extensional conditions (Decrée et al., 2008a) or to the concealed magmatic sill lying at shallow depth, or both. In that context, the structural discontinuities (thrust sheet boundaries, magmatic contacts and deformed plutons) are likely to have served as main drains (Decrée et al., 2008a). The Tamra Pliocene basin, partly overlying the Sidi Driss basin, hosts iron mineralizations that resulted from mostly in situ pedogenetic reworking with superimposed minor Late Pliocene low-temperature hydrothermal Fe, Mn, Sr, Ba, Zn and Pb mineralization (Decrée et al., 2010; Moussi et al., 2011). This late event could be correlated with the presence of galena in late veins cutting the Oued Belif granodiorite at 315 m depth. It testifies for protracted hydrothermal activity in the Nefza area, which is still currently active as shown by the thermal springs (35 °C to 70 °C: Gharbi, 1977; Zouiten, 1999) and the high regional thermal gradients of up to 100 °C·km^{-1} (Jallouli et al., 1996). Besides, in the Tamra basin, other Fe ore deposits occur in Mio-Pliocene basins, in the vicinity of magmatic rocks, as (1) in the Douahria basin, which is filled by conglomeratic/argilitic formations with numerous volcanoclastic intercalations and widespread Fe oxide impregnations. Such deposits also occur (2) at Mokta el-Hadid, in the Zouara basin, with intercalations of lacustrine carbonates, rhyodacitic flows, conglomerates – all strongly mineralized in Fe oxides, and basaltic sills – and (3) at Jebel Harsh,

Table 1
Available geochronological data for the Nefza magmatic rocks.

Massif (from east to west)	Dated material	Method	Age	References
Jebel Haddada rhyodacite	Whole rock	Rb/Sr	8.2 ± 0.4 Ma	Bellon (1976)
	Whole rock	Rb/Sr	8.6 ± 0.3 Ma	Faul and Foland (1980)
	Biotite	K/Ar	8.7 ± 0.15 Ma	Faul and Foland (1980)
Ragoubet Es-Seid rhyodacite (Oued Belif structure)	Whole rock	–	8.3 ± 0.8 Ma	Badgasarian et al. (1972)
	Whole rock	Rb/Sr	8.8 ± 0.3 Ma	Faul and Foland (1980)
	Biotite	K/Ar	8.9 ± 0.15 Ma	Faul and Foland (1980)
Ragoubet el-Alia granodiorite (Oued Belif structure)	Whole rock	K/Ar	12.9 ± 0.5 Ma	Bellon (1976)
Ain Deflaia rhyodacite	Whole rock	–	8.5 Ma	Rouvier (1977)
	Whole rock	–	11.3 Ma	Rouvier (1977)
	Whole rock	K/Ar	12.3 ± 0.5 Ma	Bellon (1976)
	Biotite	K/Ar	9.1 Ma	Rouvier (1977)
	Biotite	Rb/Sr	9.4 Ma	Rouvier (1977)
Mokta el-Hadid basalts (Zouara basin)	Whole rock	–	6.4 ± 0.15 Ma	Rouvier (1977)
	Whole rock	–	6.9 ± 0.3 Ma	Rouvier (1977)
	Whole rock	K/Ar	8.4 ± 0.4 Ma	Bellon (1976)

where the basin-filling material is strongly impregnated by Fe oxides (Negra, 1987; Rouvier, 1977).

3. Material and methods

A selection of 13 fresh magmatic rocks was made from the large collection of samples collected from 2005 to 2007 in the Nefza mining district. From the OB45 drill core located in the Oued Belif area (X = 428.247, Y = 415.393, Z = 77.94 m, with a pitch of 75° and azimuth of N110°), two samples (OB45-147 and -226) were studied. The mineralogy and texture of the rocks were determined using transmitted and polarized light microscopy. Chemical analyses (major and trace element contents; Table 2) were performed at the Geology Department of the Royal Museum for Central Africa (Jacques Navez, analyst). In addition to these new data, nineteen analyses from the literature (Appendix 1) were added to the major elements diagrams. All major element analyses were recalculated to 100% on anhydrous basis, following the recommendation of the IUGS (Le Maitre et al., 2002).

Fourteen magmatic rocks from the Nefza area were measured for their Pb isotopic composition (Table 3). They were first digested in a mixture (7/1 ratio) of suprapur HF 24 N and sub-boiled HNO_3 14 N cc. The Pb separation was achieved by successive HCl 6 N additions on pre-conditioned columns filled with an anionic resin (AG1X8). The eluted pure Pb solution was evaporated, dissolved in 100 μL of HNO_3 14 N cc, sub-boiled, evaporated and finally dissolved in 1.5 ml of HNO_3 0.05 N. A Tl solution was added to each sample and each standard to monitor and correct for mass dependent isotopic fractionation during the measurements. The sample solutions were prepared so as to obtain a beam intensity of 100 mV in the axial collector (^{204}Pb) and a Pb/Tl ratio of 4–5, matching the Pb and Tl concentrations of the NBS981 standard (200 ppb in Pb, with 50 ppb in Tl). Lead isotopes were measured using a Nu-plasma multicollector-inductively coupled plasma-mass spectrometer (MC-ICP-MS) at the 'Département des Sciences de la Terre et de l'Environnement' (DSTE — Université Libre de Bruxelles). The NBS981 standard was measured several times before each analytical session. The measurements were corrected using the mass bias of Tl and the sample-standard bracketing method (as described by Weis et al., 2006) to circumvent any instrumental drift during the analytical session. The standard analyses gave the following mean values: $^{208}Pb/^{204}Pb = 36.7141 \pm 0.021$ (2SD), $^{207}Pb/^{204}Pb = 15.4968 \pm 0.0074$ (2SD), $^{206}Pb/^{204}Pb = 16.9403 \pm 0.0071$ (2SD), which are in good agreement with long term laboratory values (n = 1000), $^{208}Pb/^{204}Pb = 36.7130 \pm 0.012$ (2SD), $^{207}Pb/^{204}Pb = 15.4950 \pm 0.004$ (2SD), $^{206}Pb/^{204}Pb = 16.9393 \pm 0.0044$ (2SD).

After acid dissolution of the sample and Sr and/or Nd separation on ion-exchange resin, Sr isotopic compositions were measured on single Ta filament and Nd isotopic compositions on triple Ta–Re–Ta filament in a TIMS (thermal ionisation mass spectrometer) VG Sector 54 from the Isotope Geology division of the Royal Museum for Central Africa, Tervuren. Repeated measurements of Sr and Nd standards showed that between-run error is better than 0.000015 (2σ). During the course of this study, the NBS987 standard yields values for $^{87}Sr/^{86}Sr$ between 0.710284 ± 0.000010 and 0.710298 ± 0.000009 (2σ on the mean of the 4 standards measured for each set of 16 samples, normalized to $^{86}Sr/^{88}Sr = 0.1194$) and the Rennes Nd standard values for $^{143}Nd/^{144}Nd$ between 0.511951 ± 0.000008 and 0.511965 ± 0.000007 (2σ on the mean of the 4 standards measured for each set of 16 samples, normalized to $^{146}Nd/^{144}Nd = 0.7219$). All measured ratios were normalized to the recommended values of 0.710250 for NBS987 and 0.511963 for Nd Rennes standard (corresponding to a La Jolla value of 0.511866). The Rb–Sr and Sm–Nd ages were calculated following Ludwig (2003). Decay constant for ^{87}Rb (1.42×10^{-11} a^{-1}) was taken from Steiger and Jäger (1977) and for ^{147}Sm (6.54×10^{-12} a^{-1}) from Lugmair and Marti (1978). Sr and Nd isotope ratios can be found in Table 3.

4. Results

4.1. Brief petrographic description

The petrographic characteristics of the Nefza magmatic rocks have been abundantly studied (e.g. Crampon, 1971; Dermech, 1990; Halloul, 1989; Halloul and Gourgaud, 2012; Laridhi Ouazaa, 1988, 1989a,b, 1990, 1996; Mauduit, 1978; Metrich-Travers, 1976; Negra, 1987; Rouvier, 1977). A brief summary of these studies, mainly those conducted by Laridhi Ouazaa (1988, 1989b, 1996), Halloul (1989) and Halloul and Gourgaud (2012) is given below.

The Oued Belif granodiorite is made up of albite (Ab_{92-97}), orthose (Or_{98}), Ti-rich biotite and quartz. The Nefza rhyodacites contain K-rich sanidine (Or_{76-71} at Ain Deflaia and Or_{76-69} at Jebel Haddada), which is more potassic at Oued Belif, plagioclase (An_{27}–An_{53}), Fe–Ti-rich biotite (with phlogopite at Oued Belif) and quartz. Two types of cordierite with distinct FeO and MgO contents (from 6 to 14.5% and from 4.5 to 9.5%, respectively) have been recognized in Ain Deflaia and Zouara. Accessory minerals are apatite, monazite, zircon, and tourmaline (with a schorlite–dravite composition, found in the cordierite-bearing rhyolite at Zouara; Halloul, 1989). The Zouara basalts contain abundant Mg-rich olivine (Fo_{79-83}, Halloul and Gourgaud, 2012; Fo_{78-69}, Laridhi Ouazaa, 1996), Ca-rich clinopyroxenes (augite and diopside), plagioclase (An_{58-67}, Halloul and Gourgaud, 2012; An_{58-37} Laridhi Ouazaa, 1996) and oxides. Voids are sometimes filled with calcite (Laridhi Ouazaa, 1996).

The rocks analyzed in this paper are shortly described below. The magmatic massifs studied here are presented from East (Jebel Haddada) to West (Zouara basin).

4.1.1. The Jebel Haddada massif

The rhyodacites were sampled in the Jebel Haddada massif, both inside the dome and in the lava flow found inside the Douharia Fe-mine, where the rock is more altered (presence of small Fe oxide grains). It is characterized by a hyalo-porphyric texture (Fig. 3A), partly devitrified (with spherolites). The phenocrysts represent 20% of total rock volume (abbreviated r.v. hereafter). They are generally euhedral and comprise plagioclase (An_{30-45};~10% r.v.), quartz (~3% r.v.), sanidine (2–4% r.v.) and biotite (±3% r.v.). The glass (±80% r.v.), sometimes perlitic, comprises biotite and plagioclase. Some samples show transparent and brown glass. Accessory minerals are zircon (mostly as inclusions within biotite), apatite and Fe–Ti oxides. When in contact with the regional host rocks (sample AHR), rhyodacite shows a fluidal texture, enhanced by biotite microliths. Pb–Ba sulfo-phosphates (SEM observation) are present as veinlets (several tens of μm wide) along the biotite cleavages in all Jabal Haddada rhyodacite samples.

4.1.2. The Oued Belif structure

Three small massifs/domes were sampled within the Oued Belif structure: (1) the Ragoubet el-Alia granodiorite, (2) the Ragoubet Es-Seid rhyodacite and (3) the Oued Arrar rhyodacite. Granodiorite has a fine-grained texture (Fig. 3B), with a crystal size of 2–3 mm. It is made up of orthoclase (35–40% r.v.), which is often albitized, albite (±30% r.v.), quartz (~20% r.v.) as isolated crystals or in a granophyric texture with orthoclase and biotite (~15% r.v.), which is partly transformed into white mica. Accessory minerals are apatite, zircon, monazite, rutile and titanite. The Ragoubet es-Seid rhyodacite contains large sanidine (up to 2 cm in length, ~12% r.v.) and biotite (up to a few mm in length, ~5% r.v.) crystals. It displays a microlitic porphyric texture (Fig. 3C, D) and locally displays a fluidal texture evidenced/enhanced by the biotite. Quartz phenocrysts often present corrosion textures. Accessory minerals are zircon (as inclusions within biotite), apatite, Fe–Ti oxide, titanite and monazite (SEM identification). The mesostasis, locally vitreous and partly altered, includes microliths of plagioclase, sanidine,

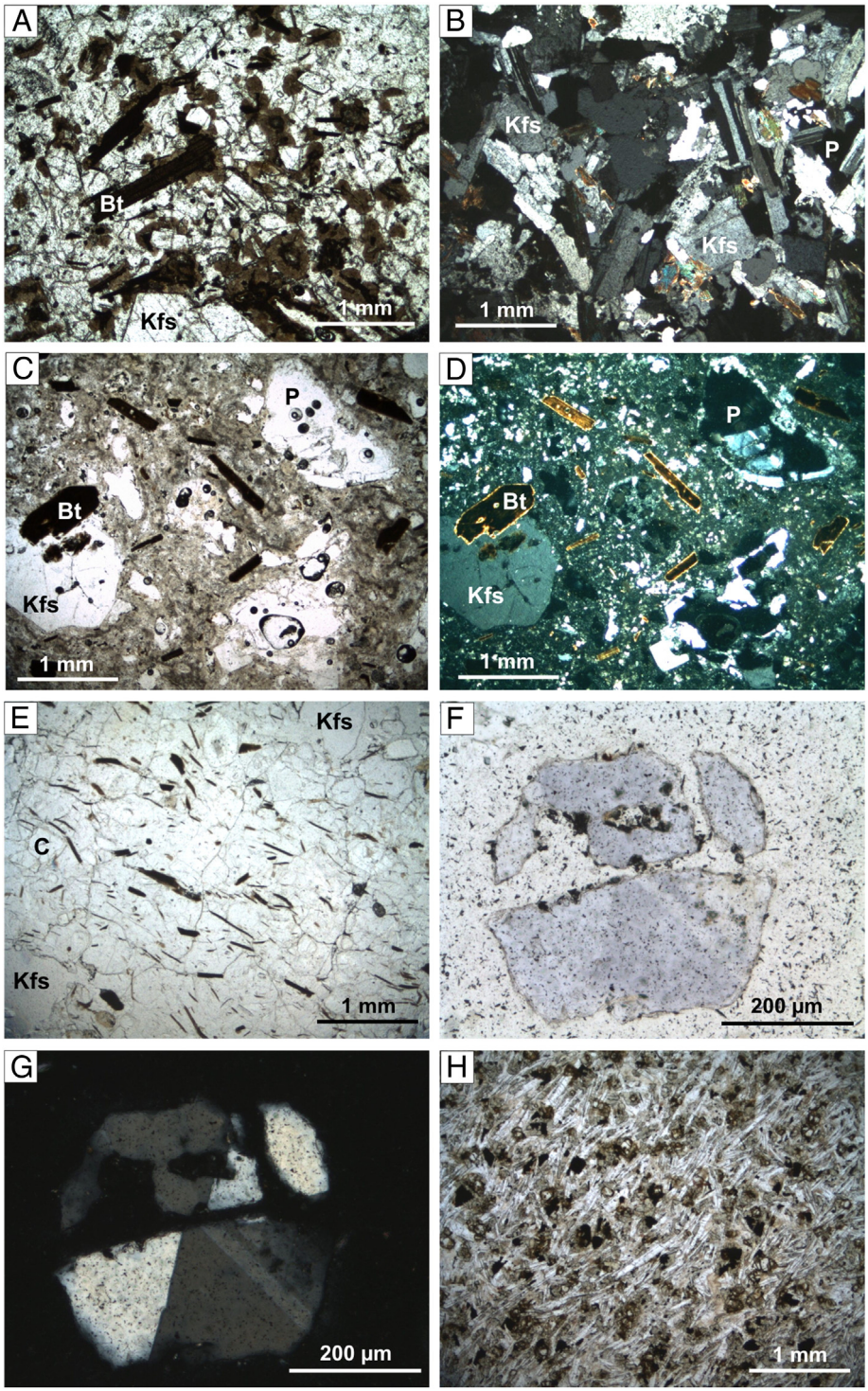

Fig. 3. Photomicrographs of the Nefza magmatic rocks using transmitted light (A, C, E, F and H) and polarized light (B, D and G). A. Jebel Haddada rhyodacite (sample HAD5): partly devitrified hyalo-porphyric texture with transparent and brown glasses, B. Ragoubet el-Alia granodiorite (Oued Belif massif, sample RA3): Fine-grained texture, C and D. Ragoubet Es-Seid rhyodacite (Oued Belif massif, sample RE2): Microlitic porphyric texture, E. Ain Deflaia rhyodacite (sample AD1): Hyalo-porphyric texture; the fluidity is enhanced by the biotite laths, F and G. Ain Deflaia rhyodacite: Cordierite with well-developed sector twinning, H. Mokta el-Hadid basalts (sample BL5): Intergranular microlitic texture; the fluidity is enhanced by the plagioclase laths. The abbreviations used are as follows: Bt for biotite, C for cordierite, Kfs for K-feldspar, P for plagioclase.

quartz and biotite. We did not find the cordierite described in the Ragoubet Es-Seid rhyodacite by Metrich-Travers (1976). The Oued Arrar rhyodacite only differs from the Ragoubet Es-Seid rhyodacite by the abundance of perlitic glass, the presence of small Ca-sulfate crystallites (several hundred micrometers large, SEM observation) and the development of a strongly weathered/altered zone (with nontronite) in the upper part of the dome.

4.1.3. The Ain Deflaia massif

The Ain Deflaia rhyodacite displays a hyalo-porphyric texture, with a fluidal texture outlined by biotite laths (Fig. 3E). Distinctive violet cordierite (up to 3 mm in size, ~5% r.v.), with a well-developed sector twinning (Fig. 3F, G) is generally fresh but can show pinitized margins and fractures. The other phenocrysts, generally euhedral, are plagioclase (~7% r.v.), quartz (4–5% r.v.),

Table 2
Major (in wt.%) and trace elements (in ppm) of the studied magmatic rocks of the Nefza district, with the corresponding A and B cationic parameters.
From Debon and Le Fort (1983)

Massif	Jebel Haddada					Oued Belif						Ain Deflaia		Mokta el-Hadid	
Description	Rhyodacitic dome			Ragoubet Bir Selem rhyodacitic flows		Ragoubet Es-Seid rhyodacite			Oued Arrar weathered rhyodacite	Ragoubet el-Alia granodiorite		cordierite-bearing rhyodacite		Basaltic flows	
Sample	HAD2	HAD3	AHR	RBS1	RBS3	RE	OB45-147	OB45-226	OAr4	RA2	RA3	AD1	AD2	BL3	BL5
SiO_2	67.74	67.75	66.70	59.07	65.92	66.82	69.70	69.38	68.75	70.28	67.49	71.13	71.14	49.28	49.23
TiO_2	0.37	0.35	0.39	0.58	0.43	0.36	0.38	0.40	0.39	0.48	0.47	0.27	0.26	1.47	1.43
Al_2O_3	15.03	15.58	16.21	23.24	17.85	14.67	15.55	15.83	15.50	16.72	16.20	14.83	14.73	17.06	17.15
Fe_2O_3 tot	2.45	2.36	2.65	4.65	2.99	3.72	2.18	2.15	2.80	0.85	2.32	2.00	1.96	9.00	8.38
MnO	0.03	0.03	0.04	0.02	0.03	0.01	0.09	0.14	0.01	0.00	0.05	0.03	0.03	0.13	0.13
MgO	0.75	0.90	1.14	1.36	0.94	1.23	0.94	0.42	1.02	0.71	0.96	0.51	0.51	6.05	5.75
CaO	2.25	2.05	1.98	0.45	1.10	0.67	1.09	1.21	0.80	0.51	0.50	1.28	1.24	9.80	10.56
Na_2O	3.22	3.47	2.66	0.88	2.47	0.77	6.51	6.28	0.91	8.10	7.68	2.91	2.94	4.44	3.86
K_2O	4.91	4.76	4.51	3.47	6.20	9.79	1.83	2.26	7.93	1.69	2.07	4.82	4.87	0.77	0.90
P_2O_5	0.19	0.18	0.08	0.21	0.25	0.06	0.21	0.22	0.24	0.19	0.17	0.26	0.25	0.26	0.26
LOI	1.73	2.51	3.76	6.86	2.55	1.38	2.23	2.63	1.91	0.93	0.94	2.61	2.65	2.58	2.52
Sum	98.67	99.95	100.12	100.80	100.72	99.48	100.69	100.90	100.26	100.48	98.85	100.65	100.58	100.84	100.18
A = "Al"	6.6	19.3	65.8	337.7	99.8	31.2	17.4	16.5	77.8	12.4	8.2	49.1	46.5	–	–
B	53.9	56.3	66.3	99.3	66.2	81.7	55.2	42.2	65.3	34.3	58.8	41.3	40.6	–	–
La	36.9	37.3	33.3	84.0	112	21.3	16.0	21.2	183	10.0	15.3	18.4	18.3	21.5	14.5
Ce	68.1	71.0	65.6	174	187	27.0	38.4	48.8	244	26.7	42.5	39.3	37.7	47.3	31.5
Pr	8.68	8.36	7.66	17.9	21.0	2.98	4.46	5.53	21.6	3.65	5.82	4.65	4.58	6.1	4.13
Nd	30.4	30.4	26.4	73.0	83.3	10.3	17.7	21.4	61.2	14.6	23.7	17.8	17.3	25.8	17.3
Sm	6.27	6.2	4.89	16.5	18.5	2	3.92	4.46	8.33	3.27	5.06	4.38	4.29	6.51	4.34
Eu	1.04	1.05	0.83	3.62	4.43	0.68	0.57	0.68	1.87	0.63	0.74	0.69	0.7	2.1	1.49
Gd	5.25	4.68	3.65	11.7	13.3	1.41	3.2	3.5	5.87	2.74	4.06	3.81	3.65	7.23	4.1
Dy	3.22	2.91	2.12	4.76	6.95	0.86	2.57	2.61	2.96	2.54	3.49	3.01	3.11	7.02	4.48
Ho	0.57	0.55	0.37	0.63	1.11	0.18	0.47	0.45	0.55	0.53	0.72	0.51	0.55	1.48	1.01
Er	1.55	1.4	1.05	1.46	2.57	0.6	1.33	1.2	1.5	1.54	1.98	1.31	1.35	4.36	2.85
Yb	1.46	1.28	1.07	1.2	1.89	0.68	1.41	1.21	1.49	1.43	1.82	1.13	1.16	4.39	2.78
Lu	0.19	0.19	0.15	0.17	0.26	0.1	0.22	0.19	0.2	0.21	0.26	0.15	0.17	0.62	0.42
Y	17.0	14.9	11.4	14.6	23.8	7.5	52.5	60.7	16.2	14.7	20.0	15.2	16.6	44.9	27.6
La_N/Yb_N	17.08	19.7	21.12	47.47	39.94	21.19	7.66	11.89	83.22	4.76	5.67	11	10.64	3.31	3.54
Eu^*/Eu	0.54	0.57	0.58	0.76	0.82	1.18	0.48	0.51	0.78	0.62	0.48	0.51	0.53	0.93	1.07
ΣREE	164	165	147	389	452	68	90	111	533	68	106	95	93	134	89
Rb	306	311	301	147	241	707	94.7	80.8	530	102	120	357	351	171	257
Sr	301	247	535	435	528	287	262	321	1289	107	130	94.6	94.5	1665	1069
Ba	469	434	461	584	592	748	206	171	1581	91.8	201	201	192	220	458
Zr	137	146	136	193	180	135	842	1041	138	185	182	98	95	211	152
Hf	3.83	4.4	4	5.7	5.2	3.69	18.41	22.9	4.05	5.4	5.3	2.9	2.9	4.9	3.6
Pb	71.45	72.7	110.19	2430	1897	14.97	1.44	10.1	119.01	3.1	135.5	35.7	36.1	8.4	7.2
Th	18.93	72.74	21.21	28.95	21.7	7.7	18.4	19.8	21.16	16.5	16.5	8.1	7.8	4.5	2.7
U	8.81	9.49	8.93	7.08	9.23	2.04	13.93	5.62	4.46	2.22	2.21	9.10	9.10	1.24	0.77
Nb	17.2	13.1	18.1	25.9	16.07	16.12	12.5	12.7	16.4	16.89	13.41	14.33	13.94	17.46	8.31
Ta	1.32	1.5	1.45	2.02	1.8	1.21	1.26	1.34	1.25	1.5	1.3	2.88	2.2	1.15	0.7
W	5.19	4.5	5.97	4.03	3.5	8.86	92.8	49.9	43.61	6.3	4	9.3	9.7	3.5	1.7

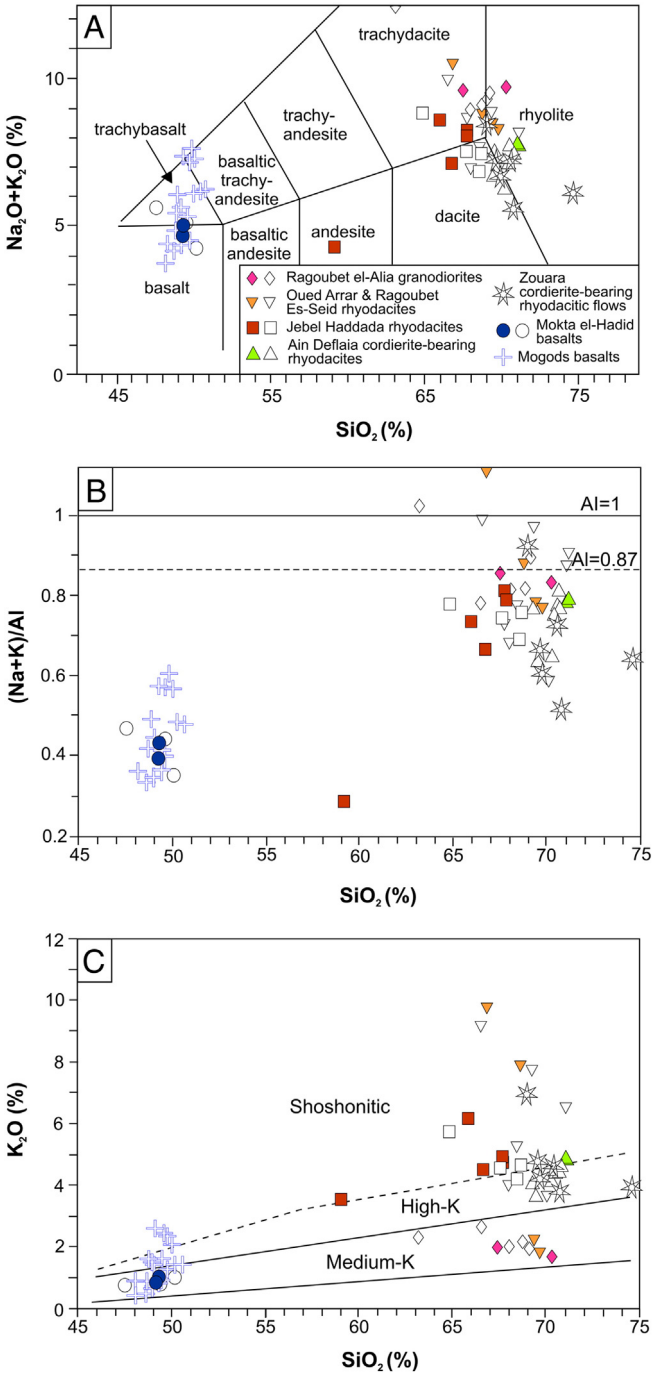

Fig. 4. Plots of the Nefza magmatic rocks in various classification/discrimination diagrams. A. TAS diagram (Le Maitre et al., 2002), B. Agpaicity: (Na + K)/Al vs. SiO_2, C. K_2O vs. SiO_2. Filled and empty symbols correspond to analyses performed for this study and taken from the literature, respectively. See the Appendix for detailed references.

sanidine (~4% r.v.) and biotite (1–2% r.v.). Apatite, zircon, titanite and opaque minerals are present as accessory minerals.

4.1.4. Zouara basin — Mokta el-Hadid location

The Mokta el-Hadid basalts present an intergranular, rarely intersertal, microlitic texture (Fig. 3H). The plagioclase laths locally enhanced the fluidity. The euhedral plagioclase phenocrysts (70% An) constitute <3% of the whole rock volume. The microlitic matrix is composed of plagioclase (~60%), augite (~20%), partly iddingsitized olivine (~15%) and undetermined opaque minerals (2–3%).

4.2. Geochemical characterization

Most of the previous works dedicated to the Nefza magmatic rocks include whole rock analyses (e.g. Crampon, 1971; Dermech, 1990; Halloul, 1989; Halloul and Gourgaud, 2012; Laridhi Ouazaa, 1989b, 1996; Mauduit, 1978; Metrich-Travers, 1976; Negra, 1987; Rouvier, 1977). Several papers (e.g.; Crampon, 1971) reported whole rock analyses of magmatic rocks from the Nefza area. These data were plotted together with our new data for comparison on Figs. 4, 5 and 6.

4.2.1. Major elements

The Nefza felsic magmatic rocks plot in the rhyolite, dacite and trachydacite fields of the TAS diagram (Fig. 4A), with in addition the RBS1 sample (Douahria basin), which has a lower silica content (58% SiO_2 vs minimum 65% SiO_2) and plot in the andesite field. For easy reference, the Nefza felsic volcanic rocks are hereafter named rhyodacites in this paper. The Ragoubet el Alia granodiorites have the chemistry of rhyolite and trachydacite. Most Nefza rhyodacites and granodiorites are characterized by an agpaitic index (AI; molar Na + K/Al) below 0.87 (Fig. 4B), which is indicative of a non-alkaline affinity, besides a strong enrichment in K (generating a shoshonitic signature for some of them, Fig. 4C). The highest values in K_2O induce a higher agpaitic index but no peralkaline mineralogy has been observed and they are probably linked to late alteration processes. The albitized granodiorites show a similar agpaitic index and lower K enrichments in the corresponding diagrams (Fig. 4B and C).

In the TAS diagram, the Nefza mafic rocks plot in the basalt and trachybasalt fields, while the Mogods mafic rocks exhibit a range of values in the basalt, trachybasalt and basaltic trachyandesite fields (Fig. 4A). They will hereafter be called “basalts” for easy reference. The Nefza basalts are moderately K-enriched, while the Mogods basalts show uneven enrichment in this element (Fig. 4C).

4.2.2. Trace elements

The chondrite-normalized REE patterns (Fig. 5) show that the Nefza granodiorites have ΣREE contents (68–106 ppm) in the lower part of the rhyodacite range (68 ppm to 437 ppm, Table 2), and lower LREE enrichment (La_N/Yb_N from 4.8 to 5.7 for the Ragoubet el-Alia granodiorite and from 7.7 to 21.2 for fresh rhyodacite). The more altered rhyodacites from Oued Arrar and Ragoubet Bir Selem have higher ΣREE (from 389 to 533 ppm) and higher La_N/Yb_N (from 39.9 to 47.5) (Table 2). Most of the Nefza felsic magmatic rocks show negative Eu anomalies ($0.49 < Eu/Eu^* < 0.58$ for fresh rhyodacites and $0.76 < Eu/Eu^* < 0.82$ for altered rhyodacites), the Ragoubet Es-Seid rhyodacite sample RE being an exception ($Eu/Eu^* = 1.2$). The Nefza granodiorites and rhyodacites exhibit primitive mantle-normalized spidergrams (Fig. 6) enriched in LILE (K, Rb, Ba, Pb) relatively to HFSE (Nb, Ta, Hf, Zr, REE). Two rhyodacites from the Oued Belif massif (OB147 & 226), characterized by abundant zircon inclusions in biotite, are less enriched in LILE and more enriched in Zr, Hf and Y. Pb, W and U are enriched in all rocks (Fig. 6; Table 2) with positive anomalies varying widely from 31 to 277 and from 350 to 956 times the Primitive Mantle, respectively (Fig. 6). The weathered and altered pyroclastic deposits from Ragoubet Bir Selem (in the Douahria Fe mine) and the Oued Arrar rhyodacite show the highest Pb anomalies reaching ~10000 and 1000 times the Primitive Mantle, respectively (Fig. 6).

The Mokta el-Hadid basalts show ΣREE contents of 89 and 134 ppm (Table 2). They are less fractionated than rhyodacites (Fig. 6C, $La_N/Yb_N = 3.3$ and 3.5) and do not exhibit significant Eu anomalies ($Eu/Eu^* = 0.93$ and 1.07). Their spidergrams are similar to those of rhyodacites (Fig. 6D), with enrichment in LILE over HFSE, W, Pb and Sr (and U in sample KKB from Crampon, 1971, 1996).

Table 3
Sr, Nd and Pb isotopic ratios of the Nefza magmatic rocks. The initial ratios (i) have been recalculated to the emplacement age (see Table 1).

Massif	Jebel Haddada					Oued Belif					Ain Deflaia		Mokta el-Hadid	
Description	Rhyodacitic dome			Ragoubet Bir Selem rhyodacitic flows		Ragoubet Es-Seid rhyodacite			Ragoubet el-Alia granodiorite		cordierite-bearing rhyodacite		Basaltic flows	
Sample	HAD 2	HAD3	AHR	RBS1	RBS3	RE	OB-145	OB-226	RA2	RA3	AD1	AD2	BL3	BL5
Age (Ma)*	8.6					8.8			12.9		9.1		6.9	
Rb (ppm)	306.3	310.5	301.4	146.8	241.5	706.7	94.7	80.8	102.1	120	357.8	350.7	171.1	257
Sr (ppm)	300.9	247.2	535.4	435.1	528.2	287.4	262	321	107	129.9	94.6	94.5	1665.4	1069
$^{87}Sr/^{86}Sr$ (measured)	0.712189	0.712023	0.710561	0.709597	0.709665	0.71111	0.70914	0.7092	0.709028	0.709197	0.719787	0.719704	0.706888	0.707071
2sigma	0.000005	0.000009	0.000008	0.00001	0.000009	0.000005	0.00001	1.1E-05	0.000011	0.000009	0.00001	0.000009	0.000006	0.000008
$^{87}Sr/^{86}Sr$ (i)	0.711829	0.711579	0.710362	0.709478	0.709503	0.710220	0.709011	0.709111	0.708522	0.708707	0.718371	0.718315	0.706859	0.707003
Sm (ppm)	6.27	6.20	4.89	16.5	18.5	2.00	3.92	4.46	3.27	5.06	4.38	4.29	6.51	4.34
Nd (ppm)	30.4	30.4	26.4	73.0	83.3	10.3	17.7	21.7	14.5	23.7	17.78	17.3	25.8	17.3
$^{143}Nd/^{144}Nd$ (measured)	0.512220	0.512211	0.512201	0.512117	0.512152	0.512243	0.51221	0.5122	0.512188	0.512208	0.512163	0.512171	0.512834	0.512808
2sigma	0.000008	0.000007	0.000009	0.000012	0.000006	0.000019	8E-06	8E-06	0.00001	0.000007	0.000007	0.000006	0.000008	0.000008
$^{143}Nd/^{144}Nd$ (i)	0.512213	0.512204	0.512195	0.512109	0.512144	0.512236	0.512198	0.512197	0.512176	0.512197	0.512154	0.512162	0.512827	0.512801
εNd (i)	−8.08	−8.25	−8.43	−10.10	−9.41	−7.62	−8.36	−8.38	−8.68	−8.28	−9.21	−9.06	3.86	3.36
$^{206}Pb/^{204}Pb$ (measured)	18.7029	18.6952	18.6953	18.6942	18.6985	18.6937	–	–	18.7460	18.7182	18.7137	18.7186	18.6467	18.6255
2SD	0.0075	0.0069	0.0075	0.0084	0.0064	0.0078	–	–	0.0125	0.0064	0.0056	0.0056	0.0105	0.0072
$^{207}Pb/^{204}Pb$ (measured)	15.6622	15.6628	15.6637	15.6597	15.6610	15.6607	–	–	15.6606	15.6641	15.6646	15.6657	15.6409	15.6414
2SD	0.0063	0.0079	0.0066	0.0075	0.0054	0.0061	–	–	0.0109	0.0059	0.0055	0.0044	0.0095	0.0064
$^{208}Pb/^{204}Pb$ (measured)	38.8563	38.8437	38.8444	38.8416	38.8342	38.8462	–	–	38.9498	38.8404	38.8339	38.8526	38.6996	38.6704
2SD	0.0171	0.0228	0.0168	0.0204	0.0143	0.0155	–	–	0.0291	0.0174	0.0154	0.0117	0.0244	0.0158
Pb (ppm)	71.5	72.7	110.2	2430	1896	15.0	–	–	3.1	135	35.7	36.1	8.4	7.2
Th (ppm)	18.9	19.3	21.2	29.0	21.7	7.7	–	–	16.5	16.5	8.1	7.8	4.5	2.7
U (ppm)	8.8	9.5	8.9	7.1	9.2	2.0	–	–	2.2	2.2	9.1	9.1	1.2	0.8
$^{206}Pb/^{204}Pb$ (i)	18.6907	18.6823	18.6873	18.6939	18.6980	18.6802	–	–	18.6464	18.7160	18.6885	18.6936	18.6321	18.6150
$^{207}Pb/^{204}Pb$ (i)	15.6622	15.6628	15.6637	15.6597	15.6610	15.6607	–	–	15.6606	15.6640	15.6646	15.6657	15.6409	15.6414
$^{208}Pb/^{204}Pb$ (i)	38.8479	38.8352	38.8382	38.8412	38.8338	38.8299	–	–	38.7116	38.8351	38.8267	38.8457	38.6827	38.6586

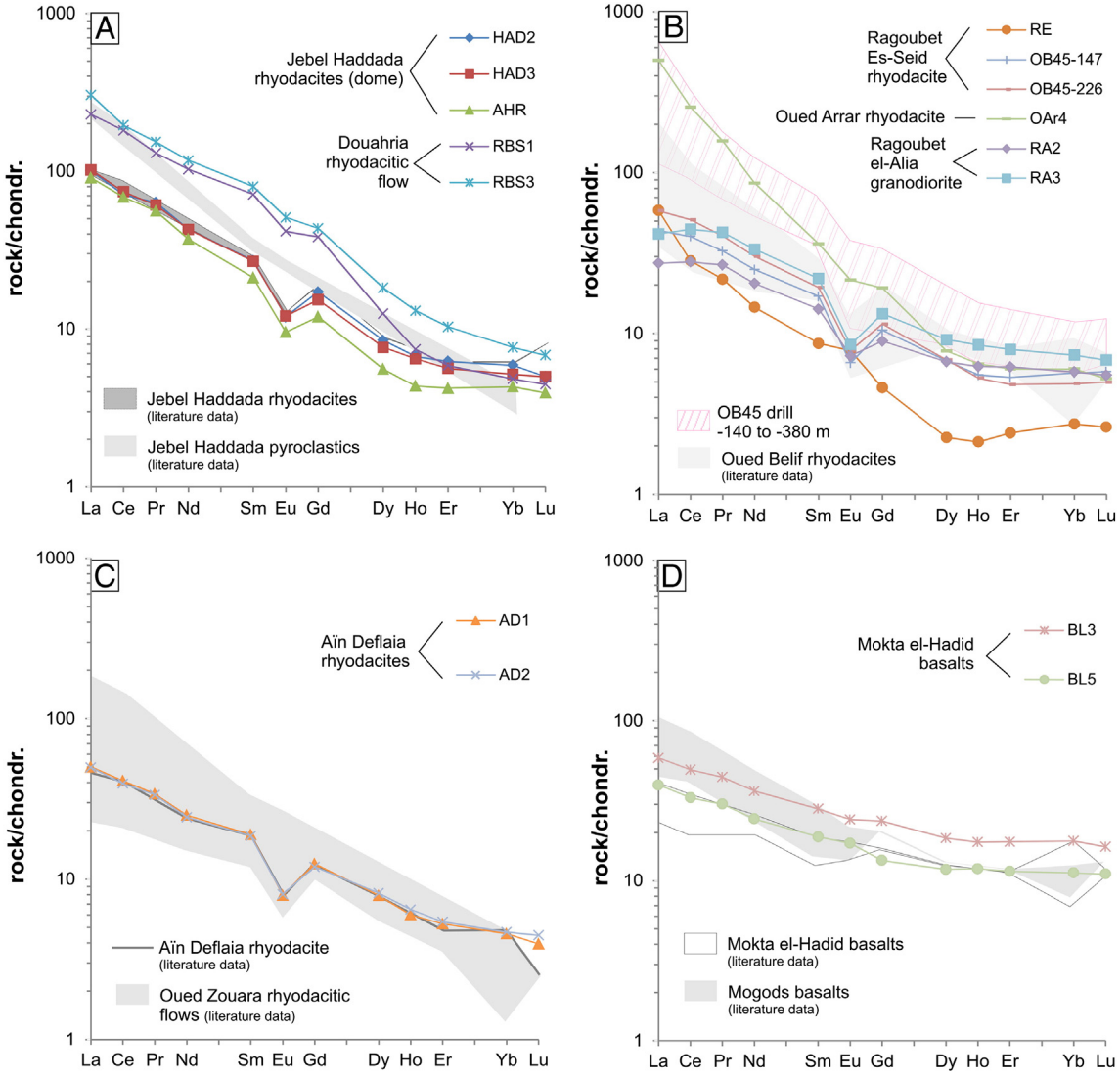

Fig. 5. REE patterns of the Nefza magmatic rocks. A: Jebel Haddada massif, B: Oued Belif massif, C: Ain Deflaia massif and Mokta el-Hadid basalts. Normalization values to the chondrites from Sun (1982) and McDonough (1990).

4.3. Isotopic data

The measured Pb, Sr and Nd isotopic ratios of the Nefza magmatic rocks have been recalculated, taking into account their emplacement ages to obtain their initial (i) isotopic compositions (Table 3) although the young age (<13 Ma) of the rocks studied here implies only a very slight increase of the isotopic compositions since their emplacement. This means that a modification of the U/Pb, Rb/Sr or Sm/Nd ratios after the magma has crystallized would induce a negligible error in the calculation of the initial isotopic ratios, including initial Pb isotopic ratios, often delicate to calculate due to subsurface mobility of U.

The Nefza felsic magmatic rocks are characterized by quite close Pb initial isotopic ratios: $^{206}Pb/^{204}Pb_{(i)}$ ratio range is 18.682–18.698 (Jebel Haddada), 18.646–18.716 (Oued Belif) and 18.688–18.694 (Ain Deflaia); $^{207}Pb/^{204}Pb_{(i)}$ ratio range is 15.660–15.664 (Jebel Haddada), 15.661–15.664 (Oued Belif) 15.665–15.666 (Ain Deflaia); $^{208}Pb/^{204}Pb_{(i)}$ ratio range is 38.834–38.848 (Jebel Haddada), 38.712–38.835 (Oued Belif) and 38.827–38.846 (Ain Deflaia). The initial lead isotopic ratio ranges for basalts are slightly lower in ^{206}Pb and ^{208}Pb, varying from 18.615–18.632 ($^{206}Pb/^{204}Pb_{(i)}$) to 15.641–15.641 ($^{207}Pb/^{204}Pb_{(i)}$) and 38.659–38.683 ($^{208}Pb/^{204}Pb_{(i)}$).

In contrast, the initial $^{87}Sr/^{86}Sr$ isotopic ratios show large variations. They vary from 0.7095 to 0.7118 for the Jebel Haddada rhyodacites and associated rhyodacitic flows, from 0.7085 to 0.7102 for the Oued Belif granodiorite and rhyodacites, from 0.7183 to 0.7184 for the Ain Deflaia massif, and from 0.7069 to 0.7070 for the Mokta el-Hadid basalts. These data are consistent with those published by Halloul and Gourgaud (2012).

All the rocks analyzed here have a narrow range of initial $^{143}Nd/^{144}Nd$ values, corresponding to negative $\varepsilon_{Nd(i)}$ (Table 3). In detail, the Jebel Haddada rhyodacitic flows show the lowest initial ε_{Nd} (−10.1 and −9.4), while the rhyodacite dome has slightly less negative values (−8.4 to −8.1). In Oued Belif, the granodiorites (ε_{Nd} = −8.7 and −8.3) have lower or similar values than the rhyodacites (ε_{Nd} = −8.4 and −7.6). The Ain Deflaia cordierite-bearing rhyodacite is within the same range (ε_{Nd} of −9.2 and −9.1). By contrast, the basalts are strikingly different and display positive values (ε_{Nd} of + 3.4 and + 3.9).

5. Discussion

5.1. Alteration and weathering processes

Petrographic observations and geochemical data show that the Nefza magmatic rocks underwent several weathering and/or alteration

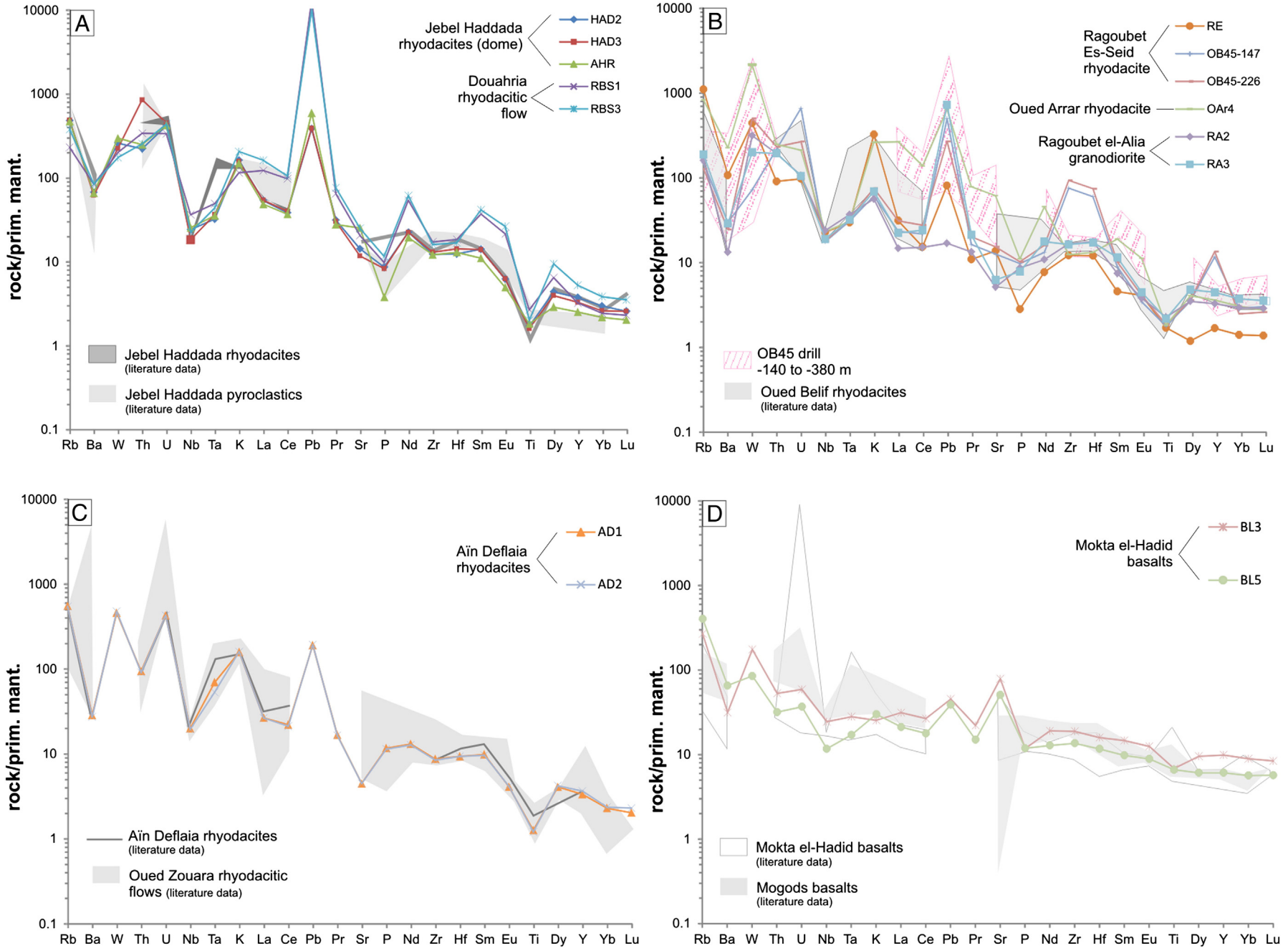

Fig. 6. Spidergrams of the Nefza magmatic rocks. A: Jebel Haddada massif, B: Oued Belif massif, C: Ain Deflaia massif and Mokta el-Hadid basalts. Normalization values to the primitive mantle from Sun and McDonough (1989).

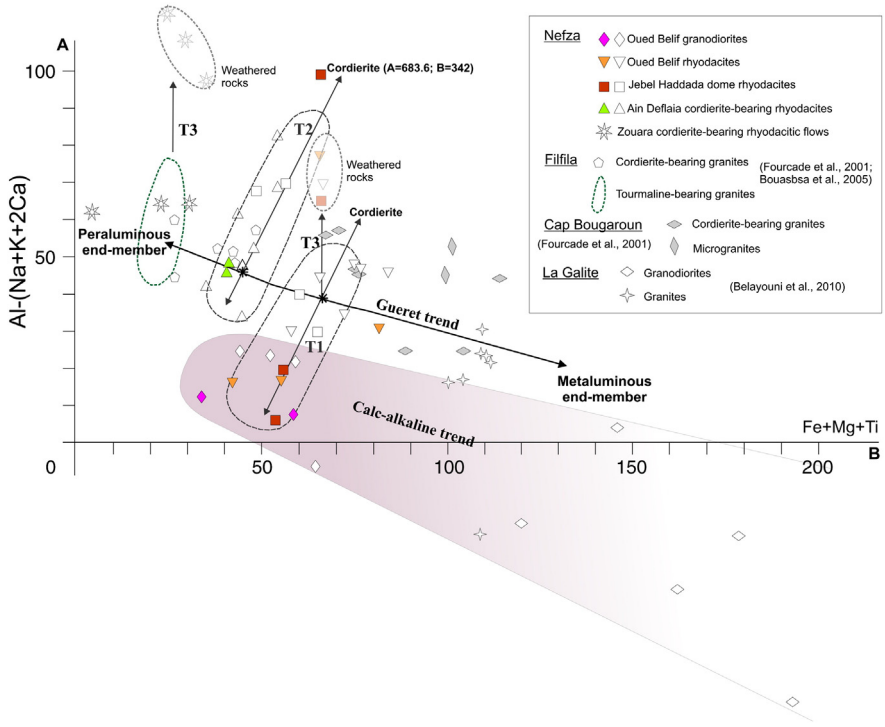

Fig. 7. Multicationic A–B Debon and Le Fort (1983) diagram for the Nefza magmatic rocks. The A and B cationic parameters are calculated in terms of millications: A = Al − (K + Na + 2 Ca) and B = Fe + Mg + Ti. The A parameter is the classical alumina index. B is directly proportional to the weight content of dark minerals in common granitic rocks. For comparison purposes, are also plotted the granites and granodiorites from the La Galite island (data from Belayouni et al., 2010), the cordierite- and tourmaline-bearing granites from the Filfila massif (NE Algeria; Fourcade et al., 2001; Bouabsa et al., 2005), and the cordierite-bearing granites and microgranites from the Cap Bougaroun massif (NE Algeria; Fourcade et al., 2001). The Gueret trend illustrates the mixing of metaluminous calc-alkaline and peraluminous magmas defined in the Variscan Millevaches massif, France (Stussi and Cuney, 1993). T1, T2 and T3 trends correspond to cordierite fractionation, cordierite accumulation and alteration/weathering, respectively. The black asterisks represent the initial compositions of the magmas before cordierite accumulation or fractionation. Filled and empty (or light grey) symbols correspond to analyses performed for this study and taken from the literature, respectively. See the Appendix for detailed references.

processes. (1) Late-magmatic processes at Ragoubet el-Alia induced the albitization of the K-feldspar in the granodiorite. (2) All the Nefza magmatic rocks are variously enriched in Pb (1.4 to 2430 ppm), W (1.7 up to 92.8 ppm) and U (0.77–13.93 ppm) presumably due to late- or post-magmatic circulation of hydrothermal fluids. In the Jebel Haddada and Douahria rhyodacites, Pb enrichment is marked by the presence of late hydrothermal Pb–Ba sulfo-phosphate-bearing veinlets. At Oued Arrar, the rhyodacite is strongly enriched in W as shown by the presence of hydrothermal Ca-sulfates suggesting that the fluids were enriched at depth on contact with Triassic formations, where Ca-sulfates and muscovite (potentially W-enriched; Krauskopf, 1970) are abundant (Negra, 1987). (3) Eventually, the Nefza rocks were also weathered. This is conspicuous in the rhyodacite flows at Douharia and at Oued Arrar, where a nontronite-rich zone formed in the upper part of the rhyodacite dome. In addition, these rocks present strong REE enrichment ($389 < \sum REE < 553$ ppm), especially in LREE ($40 < La_N/Yb_N < 83$), which can be related to the occurrence of secondary supergene monazite.

The basalts were less affected by the alteration and mineralization processes, probably due to their younger age, most alteration

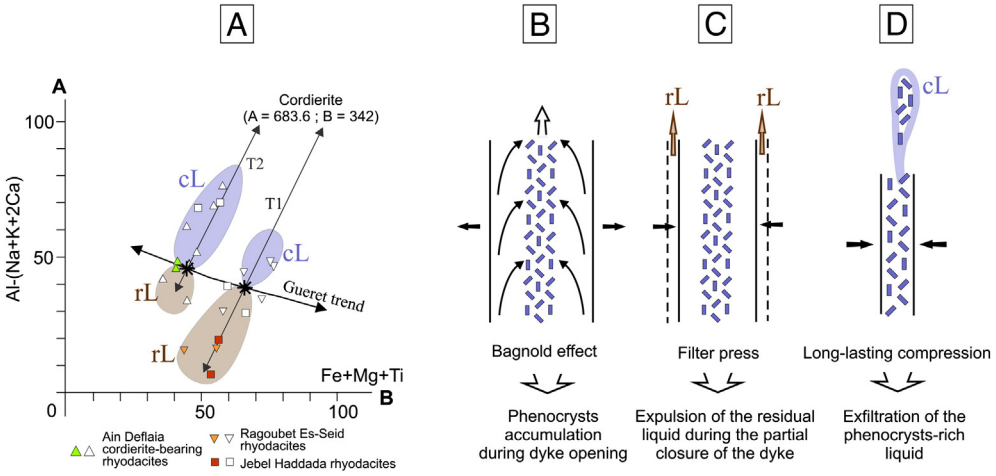

Fig. 8. Bagnold effect and filter-press processes explaining some of the chemical variations observed in the Debon and Le Fort (1983) A–B diagram for the Nefza rhyodacites (see text for detailed explanation). Filled and empty symbols correspond to analyses performed for this study and taken from the literature, respectively. See the Appendix for detailed references.

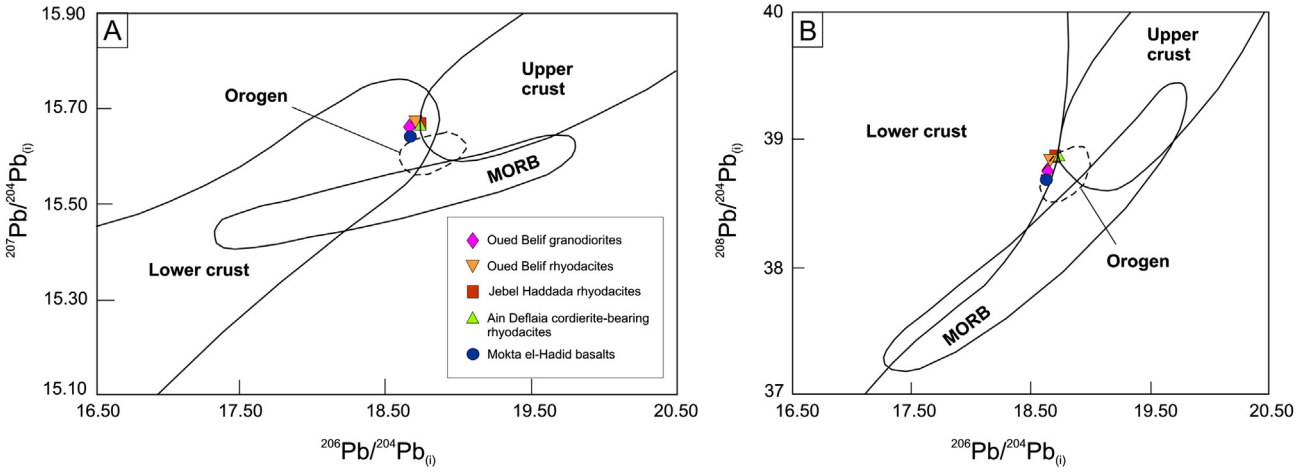

Fig. 9. Initial Pb isotopic ratios for the Nefza magmatic rocks in the $^{207}Pb/^{204}Pb$ vs. $^{206}Pb/^{204}Pb$ and $^{208}Pb/^{204}Pb$ vs.$^{206}Pb/^{204}Pb$ diagrams, with the major terrestrial reservoirs defined by Zartman and Doe (1981).

events having occurred earlier, during the post-magmatic stages of felsic magmatism. However, they show strong Sr enrichment (1069–1665 ppm), which could be related to the circulation of late shallow-depth fluids which were enriched on contact with the Zouara host-rocks, which comprise carbonates and sulfates.

5.2. Discrimination of the magmatic processes using the Debon-Le Fort diagram

The multi-cationic A–B diagram (A = Al − (K + Na + 2 Ca) and B = Fe + Mg + Ti) of Debon and Le Fort (1983) was used to compare the

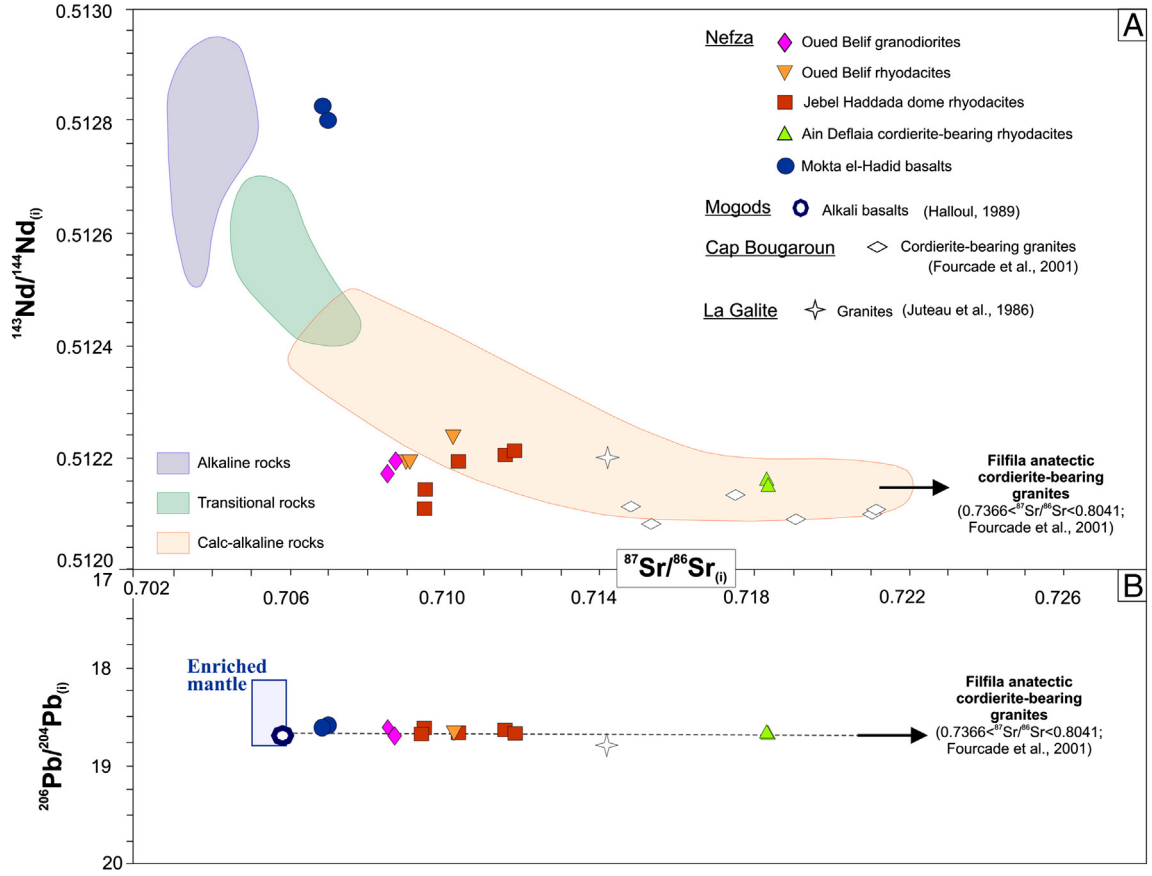

Fig. 10. A. Sr–Nd isotopic diagram for the Nefza magmatic rocks. The data for the La Galite granites (Juteau et al., 1986) and for the Cap Bougaroun and the Filfila cordierite-bearing granites (Fourcade et al., 2001) are given for comparison. The alkaline, transitional and calc-alkaline fields were defined by Maury et al. (2000) for the Mediterranean margin magmatic rocks. B. Correlations between the initial Sr and Pb ($^{206}Pb/^{204}Pb$) isotopic ratios for the Nefza magmatic rocks. The Mogods alkali basalts, the La Galite granites and the Filfila anatectic granites are plotted for comparison (data from Halloul, 1989; Juteau et al., 1986 and 堪aFourcade et al., 2001).

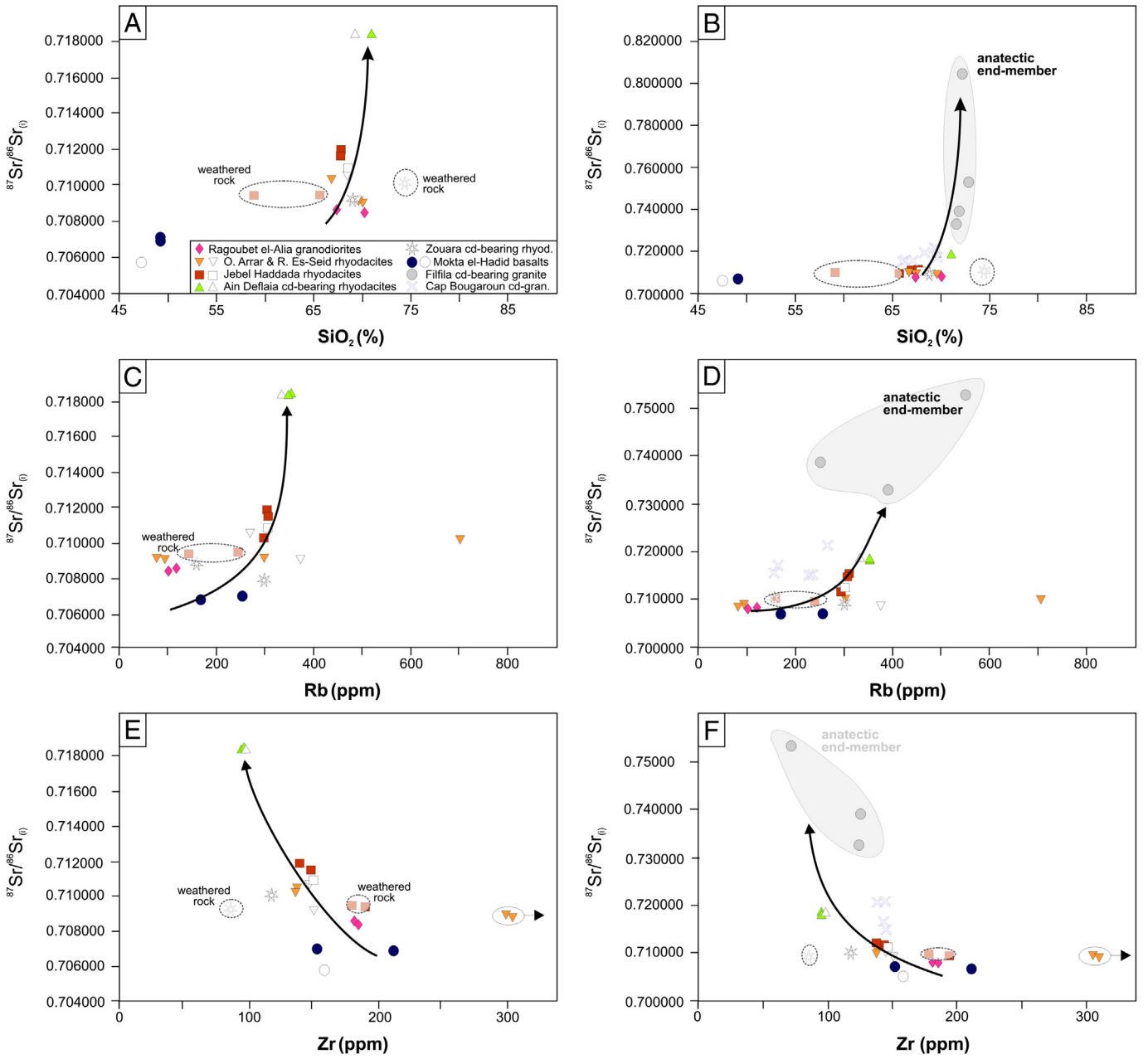

Fig. 11. Correlations between the initial $^{87}Sr/^{86}Sr$ isotopic ratios and the contents in SiO_2 (wt.%) and in some trace elements (Rb and Zr, in ppm) for the Nefza magmatic rocks (A,C,E) and for the Filfila anatectic cordierite-bearing granites and the Cap Bougaroun cordierite-bearing granites (B,D,F; from Fourcade et al., 2001). Filled and empty symbols correspond to analyses performed for this study and taken from the literature, respectively. See the Appendix for detailed references.

Nefza magmatic rocks to other magmatic suites of the same area: the granites and granodiorites from La Galite island (60 km north of Tabarka; Belayouni et al., 2010) and the Langhian cordierite/tourmaline-bearing granites and microgranites from the Filfila and Cap Bougaroun massifs (180–230 km west of Nefza in Algeria; Bouabsa et al., 2005; Fourcade et al., 2001). The latter define a trend interpreted as resulting from the mixing of metaluminous calc-alkaline and peraluminous magmas (Bouabsa et al., 2005; Fourcade et al., 2001). This trend was called the "Gueret trend" by Stussi and Cuney (1993) in their study of the Variscan Millevaches massif in the French Massif Central. Since the A parameter of the diagram is sensitive to alteration and weathering (leaching of Na, K and Ca), the weathered rocks (vertical trend T3 on Fig. 7) were plotted within an ovoid faded field (emphasized by a dashed line) but were not taken into account in the interpretation of the magmatic processes (Fig. 7).

The Nefza felsic magmatic rocks exhibit two main trends (Fig. 7): (1) the Oued Belif granodiorites have an elongated trend running roughly parallel to the calc-alkaline trend, very much like the La Galite granodiorites trend; the dispersion of the samples along the A axis can be related to the late-magmatic alteration (albitisation and transformation of biotite into white mica); (2) most rhyodacites are located in the vicinity of the "Gueret trend," suggesting that they result from metaluminous to peraluminous magma mixing. The Ain Deflaia cordierite-bearing rhyodacites are close to the peraluminous end-member of the diagram, represented by the Filfila anatectic granites (Bouabsa et al., 2005), while the position of the Oued Belif and Haddada rhyodacites along the "Gueret trend" is indicative of a less important crustal contribution. The Nefza rhyodacites exhibit three additional trends (T1, T2, T3; Figs. 7 and 8). The upper part of trends T1 and T2, above the "Gueret trend", could represent the accumulation of

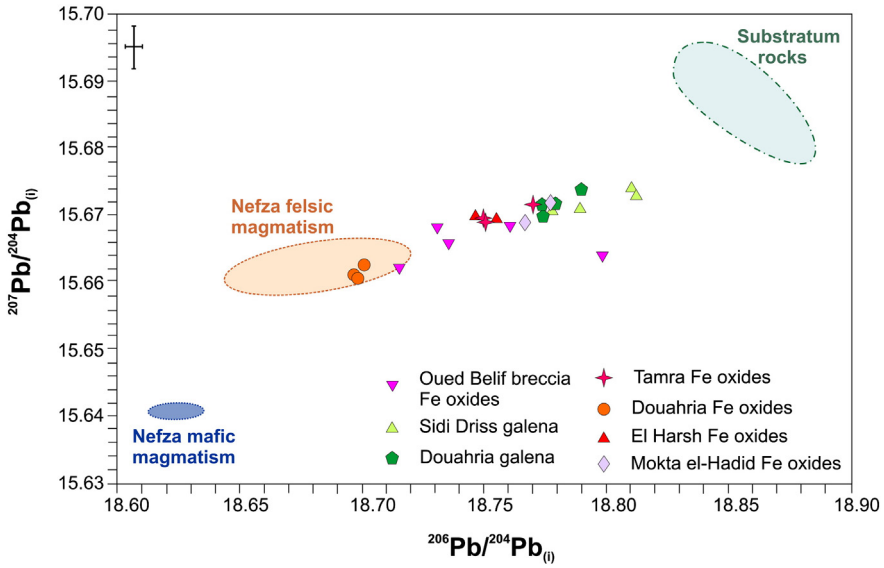

Fig. 12. Pb isotopic ratios for igneous rocks, mineralizations and three sedimentary substratum rocks from the Nefza area (Decrée et al., 2008a,b) plotted on a $^{207}Pb/^{204}Pb$ vs. $^{206}Pb/^{204}Pb$ diagram. All the Pb isotopic ratios are recalculated at 5.5 Ma, which is an estimated age for most of the Pb–Zn–Fe mineralizations in the area. The error bar represents the mean for the standard deviations.

cordierite (~10% accumulated cordierite) while their lower part, below the "Gueret trend", could reflect the fractionation of cordierite (5–10% of fractionated cordierite). The accumulation and/or fractionation of cordierite can occur in any magma resulting from the mixing of peraluminous and metaluminous end-members, as can be seen all along the "Gueret trend". Considering the small volumes of the magmatic bodies studied here, this can be achieved through the Bagnold effect and filter-press processes occurring within the feeding dykes, as proposed for example in the Tin Zebane dyke swarm of Algeria (Hadj et al., 1998) and in the Motru dyke swarm of Romania (Nkono et al., 2006). As illustrated in Fig. 8, the Bagnold effect induces an accumulation of phenocrysts (here, cordierite) in the central part of the opening feeding dyke and a concentration of a slightly fractionated residual liquid along the margins of the dyke. This liquid, which is found to be depleted in cordierite (lower part of T1 and T2 trends) can be expelled with a filter press during the partial closure of the dykes, when the magmatic feeding of the dyke decreases. Finally, the long-lasting compression of the feeding dyke can result in the exfiltration of the phenocryst-rich liquid (cL), which is found to be enriched in cordierite (upper part of trends T1 and T2). The rL and cL liquids can be collected in an intermediate magmatic chamber, represented by the magmatic bodies now at the surface, with variable mixing ratios of these liquids.

5.3. Isotopic composition and magmatic sources

In the Pb isotopic diagrams (Zartman and Doe, 1981; Zartman and Haines, 1988), the initial Pb isotopic composition of the Nefza magmatic rocks (Fig.9) defines narrow fields at the intersection of the lower and upper crust fields, and very close to the Orogen reservoir.

The Sr isotopic compositions of the Nefza rocks (Table 3) present a wide range of values between 0.7068 and 0.7182, but each massif has a distinct composition, in contrast with Nd and Pb isotopes, which are much more homogeneous (Fig. 10A, B). In the $^{87}Sr/^{86}Sr$ vs. $^{206}Pb/^{204}Pb$ diagram (Fig. 10B), the linear trend extends from an enriched mantle composition, locally represented by the Mogods alkali basalts ($^{87}Sr/^{86}Sr = 0.7057$; Halloul, 1989) to an old continental crust, locally represented by the Filfila anatectic granites ($0.7366 < {}^{87}Sr/^{86}Sr < 0.8041$; Fourcade et al., 2001). Along this mixing line, the transitional basalts of Mokta el-Hadid are very similar to the enriched mantle pole, suggesting that they were only slightly affected by crustal contamination. On the other hand, the Ain Deflaia cordierite-bearing rhyodacites have high Sr isotopic ratios, which are found to be close to those of the old crustal pole. However, the Filfila cordierite granites have even higher values suggesting either that the Ain Deflaia rhyodacites are not pure crustal products or that the (meta) sedimentary source was heterogeneous. The Oued Belif granodiorites — rhyodacites and the Jebel Haddada rhyodacites have intermediate Sr isotopic compositions that are indicative of variable crustal/sedimentary proportions, as also suggested by Maury et al. (2000). The correlations (hyperbolic curves) between initial Sr isotopic compositions and the content of SiO_2, Rb and Zr contents (Fig. 11A to F) and the dispersion of the Nefza rocks along a trend evolving towards the Filfila anatectic granite (Fig. 11B, D and E) further suggest mixing/crustal contamination.

The homogeneous Pb isotopic compositions of all the Nefza magmatic rocks could also be explained by the high to extreme Pb content (35 to 135 ppm for most rocks, with values up to 2430 ppm for the Ragoubet Bir Selem rhyodacitic flows; see Table 2 and Fig. 6), which may have buffered the Pb isotopic signature. Indeed, since the substratum rocks are characterized by quite homogeneous Pb isotopic compositions (see below), the interaction of the magmatic rocks with their surrounding host-rocks through Pb-rich hydrothermal fluid circulations might have rapidly shifted the Pb isotopic compositions of the Nefza magmatic rocks at a higher common Pb isotopic ratio (buffering).

Nd isotopes (Fig. 10A) strongly discriminate the Nefza basalts with positive ε_{Nd} values (+3.2 and +3.7) from the felsic rocks that have distinctively negative ε_{Nd} values (from −7.8 to −10.3). The Nd signature of the basalts is in agreement with the Pb isotopes and indicates an enriched mantle source with little, if any, crustal contribution.

The initial Sr isotopic values (0.7068–0.7070) of the Mokta el-Hadid basalts are relatively high for alkali basalts and could be related to the effect of late fluids at shallow depths. This explains their position to the right of the circum-Mediterranean alkaline basalt field (Fig. 10). The negative ε_{Nd} of the felsic rocks can hardly be attributed to superficial (shallow hydrothermal) fluids because of the general immobility of REE in these conditions. REE can be mobile in greenschist conditions but this is displayed in REE diagrams (Ennih and Liégeois, 2008). The mixing between the mantle and crustal reservoirs in the Nefza district thus occurred at depth; this process was efficient as the Nd isotope signature varies only slightly, even in cordierite-bearing granites. This can be explained by the fact that the cordierite was generated at shallow depth through the digestion of country rocks, as in the case of the Temaguessine pluton (Abdallah et al., 2007); such a process, at pluton

Table 4
Pb isotopic ratios of the sedimentary rocks of the substratum and of various iron oxides and galenas. The initial ratios have been recalculated the emplacement age of most of the Pb–Zn–Fe mineralizations, at about 5.5 Ma.

Description	Substratum — Ed Diss marls		Substratum — Ypresian carbonate	Substratum — Albian limestone	Oued Belif breccia — ferruginous matrix (Decrée et al., 2013)					Tamra iron oxides		
Sample	ED1	ED2	MA1	CA1	BC04/1	Brèche	DV3	DV4	OG2	CP04/19	CP04/20 ter	CP04/36
$^{206}Pb/^{204}Pb$ (measured)	18.8566	18.9116	18.8605	19.2557	18.8014	18.7156	18.7603	18.7309	18.7352	18.7598	18.7508	18.7701
2SD	0.0083	0.0059	0.0065	0.0079	0.0083	0.0067	0.0065	0.0144	0.0067	0.0049	0.0095	0.0086
$^{207}Pb/^{204}Pb$ (measured)	15.6936	15.6802	15.6907	15.7164	15.6642	15.6625	15.6685	15.6682	15.6657	15.6700	15.6691	15.6721
2SD	0.0069	0.0046	0.0055	0.0067	0.0068	0.0065	0.00611	0.01554	0.00632	0.0048	0.0077	0.0068
$^{208}Pb/^{204}Pb$ (measured)	38.9718	38.8888	38.9620	38.9992	38.8373	38.8444	38.8520	38.8519	38.8436	38.8592	38.8521	38.8659
2SD	0.0196	0.0143	0.0155	0.0175	0.0177	0.0157	0.0277	0.0347	0.0165	0.0126	0.0175	0.0193
Pb (ppm)	26.1	3.4	7.8	5.2	271	2403	577	2950	342	1011	12136	6637
U (ppm)	4.0	1.8	2.9	5.6	13.0	5.9	140	413	39.5	2.1	2.0	1.2
Th (ppm)	9.2	0.3	6.0	3.4	150	223	4	19.6	8.1	8.2	1.2	8.7
$^{206}Pb/^{204}Pb$ (at 5.5 Ma)	18.847	18.880	18.838	19.190	18.798	18.715	18.760	18.731	18.735	18.750	18.751	18.770
$^{207}Pb/^{204}Pb$ (at 5.5 Ma)	15.694	15.680	15.691	15.716	15.664	15.662	15.669	15.668	15.666	15.670	15.669	15.672
$^{208}Pb/^{204}Pb$ (at 5.5 Ma)	38.965	38.887	38.947	38.986	38.826	38.843	38.852	38.852	38.844	38.859	38.852	38.866

scale, affects only some mobile elements (such as alkalis and Sr) and not others (such as REE). As a whole, the Nefza felsic rocks display an Sr–Nd signature, which is similar to that of the Miocene magmatic rocks in the Maghreb area (Maury et al., 2000).

5.4. Geodynamics

The Nefza Late Miocene magmatism within the Atlas collision belt was ultimately caused by the partial melting of the North Africa SCLM (sub-continental lithospheric mantle) and is usually ascribed to a lithospheric delamination developed in relation with a "Tethysian slab roll-back" (Coulon et al., 2002; Maury et al., 2000), which also influenced the formation of the Tellian and Atlas Zones (e.g. Gelabert et al., 2002; Michard et al., 2006). The enrichment of the SCLM is attributed to subduction-related metasomatism that occurred during Variscan and/or Pan-African orogenies. Such metasomatism explains both the apparent "subduction-related" geochemical signature and the old isotopic signature of this Late Miocene magmatism.

A detailed analysis reveals that several alternative models exist. They give varying importance to major processes such as the subduction of the Tethyan Ocean, the opening of the Provençal–Algerian and Tyrrhenian back-arc basins (e.g., Carminati et al., 1998; Gueguen et al., 1998; Handy et al., 2010; Mascle et al., 2004) and the heterochronous accretions of island arcs from the Oligocene to the Quaternary (Rekhiss, 2007; Tricart et al., 1994). Detailing all these models is beyond the scope of this paper. What is of concern here is that shear zones and associated lineaments inherited from the Variscan orogeny were transtensionally reactivated during the Alpine orogeny (Piqué et al., 2002) and controlled the Late Cenozoic magmatic and hydrothermal events (Fig. 1B). Basalt dykes of mantle origin were also emplaced along these lineaments (the Mokta el-Hadid basalts along the NE–SW Ghardimaou-Cap Serrat fault and the Mogods basalts along the WSW–ENE fault; Talbi et al., 2005), demonstrating that these fault zones are of lithospheric scale. Bearing in mind that no oceanic subduction occurred beneath the African continent during the period considered (Jolivet, 2008), we support a model of reactivation of a former passive margin in post-collision setting and of metacratonic character (Liégeois et al., 2013). In such a setting, planar lithosphere delamination along these deep-seated reactivated faults, rather than regional roll-back, allegedly triggered the northern Tunisian magmatism. This kind of shear zone reactivation can generate large batholiths (De Waele et al., 2006; Liégeois et al., 1998, 2003; Shang et al., 2007, 2010; Toummite et al., 2013), late high-level plutons and dykes at the end of this period (Abdallah et al., 2007; Azzouni-Sekkal et al., 2003; Duchesne et al., 2013) or even intraplate volcanism (Liégeois et al., 2005) at the climax of the post-collisional period.

5.5. Relationship between regional magmatism and mineralizations

In the Nefza mining district, magmatic rocks and mineralizations were controlled at the same time by the same set of regional fault zones, inherited from the Variscan orogeny (maybe also from the Pan-African orogeny) and reactivated during the Alpine orogeny. Magmatism and mineralizations are indeed coeval (as is the IOCG mineralization related to the Oued Belif breccia; Decrée et al., 2013) or at least occurred within a narrow time frame (e.g. the Sidi Driss and Douahria sedex Pb–Zn deposits; Decrée et al., 2008a). Constraining the relationships existing between these two kind of events is thus of paramount importance.

The Pb isotopic composition of the various regional mineralizations is plotted in the $^{207}Pb/^{204}Pb$ vs. $^{206}Pb/^{204}Pb$ diagram and compared to those of the Nefza magmatic rocks and of the sedimentary substratum (marls and limestones) (Fig. 12, Table 4). This diagram shows that the mineralizations display a trend extending between the Nefza magmatic rocks and their substratum. This suggests that the lead found in the mineralizations does not only come from magmatic rocks but also from the rocks surrounding the ore deposits. A likely process is the leaching of the lead from these formations by regional fluid circulations, the structural discontinuities appearing along these Pb "reservoir" rocks (thrust sheet boundaries and magmatic contacts) serving as main drains (Decrée et al., 2008a). The Pliocene Fe oxides from the El Harsh and Tamra mines are characterized by less radiogenic isotopic compositions than the Messinian galena from the nearby Sidi Driss and Douahria sedex Pb–Zn deposits. This suggests that the presence of Fe-ore bears evidence to the mixing of two distinct lead reservoirs in subsurface environment: (1) the magmatic rocks and (2) the sedex mineralizations, both reservoirs being leached along the structural discontinuities, as suggested above. The hydrothermal activity resumption leading to such mixing could be attributed to the Late Mio-Pliocene regional extensional events that favor crustal thinning and high geothermal gradients. Extreme cases can be found in the Douahria Fe ore deposits, which have isotopic composition comparable to that of rhyodacite, suggesting that the main Pb source is the magmatic rocks themselves, without any sedimentary contribution. Preserved cinerites (even though altered, samples BSR1 and 3 from Ragoubet Bir Selem) have actually been found in the Douahria Fe mine.

On a broader scale, the Nefza ore deposits and the Pb–Zn–Hg–Cu–Ag–Au showings and deposits occurring in the vicinity of this district (e.g. Hg

Douahria iron oxides			El Harsh iron oxides		Mokta el-Hadid iron oxides		Sidi Driss galena				Douahria galena			
CH2	CH3	CH4	DH2	DH3	BL4	BL5m	CI3	SD2	SD2a	SD4/5	DSU1	DSU5	DSU6	DSU4
18.6986	18.6979	18.7009	18.7557	18.7465	18.7766	18.7667	18.8196	18.7785	18.7891	18.8121	18.7892	18.7775	18.7736	18.7717
0.0058	0.0072	0.0064	0.0062	0.0063	0.0061	0.0072	0.0061	0.0095	0.0088	0.0099	0.0071	0.0105	0.0061	0.0075
15.6606	15.6607	15.6625	15.6696	15.6702	15.6718	15.6691	15.6737	15.6707	15.6710	15.6731	15.6740	15.6716	15.6719	15.6704
0.0053	0.0067	0.0055	0.0143	0.0066	0.0050	0.0064	0.0059	0.0074	0.0077	0.0087	0.0060	0.0076	0.0063	0.0064
38.8346	38.8346	38.8402	38.8653	38.8691	38.8681	38.8557	38.8658	38.8476	38.8530	38.8617	38.8824	38.8721	38.8879	38.8571
0.0166	0.0180	0.0149	0.0440	0.0178	0.0129	0.0158	0.0180	0.0196	0.0213	0.0239	0.0210	0.0216	0.0146	0.0174
1848	1354	905	375	1132	3003	1071	–	–	–	–	–	–	–	–
4.9	4.7	3.4	2.8	3.5	50.3	11.0	–	–	–	–	–	–	–	–
6.7	9.3	6.6	7.1	3.0	0.9	1.8	–	–	–	–	–	–	–	–
18.699	18.698	18.701	18.756	18.746	18.777	18.767	18.810	18.778	18.789	18.812	18.789	18.777	18.774	18.772
15.661	15.661	15.662	15.670	15.670	15.672	15.669	15.674	15.671	15.671	15.673	15.674	15.672	15.672	15.670
38.835	38.835	38.840	38.865	38.869	38.868	38.856	38.866	38.848	38.853	38.862	38.882	38.872	38.888	38.857

mineralization at Ain Allega); Pb–Zn MVT along the Ghardimaou-Cap Serrat shear zone (Gharbi, 1977; Abidi et al., 2010); Pb–Zn–Au showings at Ras Rajel (Albidon Limited, 2004); pyrite, chalcopyrite and sulfosalts assemblage in La Galite Island (Slim-Shimi et al., 1990) may constitute a metallogenic province that fits the context of the inherited crustal or lithospheric-scale fault reactivation. The spatial and temporal association of the mineralizations with Miocene magmatism can be very tight, in the same way as the Pb–Zn–Au enrichment and the dacitic breccia at Ras Rajel. Similarly, at La Galite Island, the Bi–Sb–Cu mineralizations are related to high-temperature fluid circulations due to the intrusion of granodiorites and granites (Slim-Shimi et al., 1990). As shown in this study, the La Galite felsic magmatic rocks define the same geochemical trend as the Nefza rhyodacites and granodiorites (see Figs 7 and 10) and belong to the same geodynamic/magmatic context. This metallogenic province can be extended to the whole Eastern Maghrebide belt (Decrée et al., 2013), which displays numerous polymetallic deposits connected to Miocene magmatic rocks within the same geodynamic context. For instance, (1) Au–Sb–Cu–W and mesothermal Cu–Pb–Zn mineralizations are related to the Edough Miocene metamorphic core complex (Aïssa et al., 1998, 2001), (2) the flysch in the Ain Barbar area hosts Cu–Pb–Zn mesothermal vein mineralization associated with Langhian subvolcanic magmatism (Marignac, 1985, 1988a,b), (3) Fe-deposits are related to microgranite bodies intruding the Kabylian Flysch in the Cap de Fer area (Algeria), and (4) Fe skarn mineralization is associated with the Nador magmatic center in the Rif segment of the Maghrebides (Rhoden and Ereño, 1961). It is also worth noting that in the Betics a Late Tortonian metallogenic event is closely spatially and temporarily related to the late stages of calc-alkaline volcanism (Hernandez et al., 1987 and references therein), which is not unlike what happened in the Nefza district.

6. Conclusions

The activity of the Upper Miocene Nefza magmatic province (Northern Tunisia) began during the Serravallian–Tortonian with the emplacement of intermediate and felsic rocks whose origin is mainly the old continental sedimentary crust (in line with their peraluminosity) with subordinate contribution from an enriched mantle. It ended during the Messinian with the extrusion of basalts originating from this enriched mantle source. All of these magmatic rocks were altered at shallow levels through fluid interactions that modified the contents of incompatible water-mobile elements (LILE), including Sr isotopes. On the contrary, Nd and Pb isotopes were not (or only very slightly) affected by this late event. Immobility of Nd isotopes was expected, unlike that of Pb isotopes. This can be explained by (1) the young age (<13 Ma) of the rocks studied (the potential mobility of U has poor incidence on the calculation of Pb initial ratios) and (2) by the high Pb concentrations of all the rocks studied (from several dozens of ppm up to more than 2000 ppm in some cases).

Miocene Nefza magmatism developed in a post-collisional setting. Such a geodynamic environment is conducive to the remelting of pre-existing sources, especially the most enriched and fusible ones (Liégeois et al., 1998). The oldest form of (Serravallian to Tortonian) Nefza felsic magmatism results from the mixing at depth of an enriched mantle-derived calc-alkaline magma with a predominant peraluminous crustal melt. Such mixing is identified in the major and trace elements as well as in the Pb–Nd isotopes. The younger Messinian basalts essentially derive from the enriched mantle source and are nearly devoid of crustal participation.

The enrichment of the mantle source, including radiogenic isotopes that are variously present in the different Nefza magma batches, implies an old subduction event, most probably during the Variscan orogeny but maybe also during the Pan-African orogeny, leading to metasomatic K- and LILE-enriched pods in the lithospheric mantle, prone to remelting in post-collisional conditions (Liégeois et al., 1998), including the former passive margin side (metacratonization; Liégeois et al., 2013). Sr isotopes demonstrate an additional upper crust input in the Nefza magmas close to their emplacement depth, which explains the appearance of magmatic cordierite in some facies. Variation of the modal abundance of cordierite can be linked to the magma movements in the feeding dykes (Bagnold and filter-press effects).

The Pb isotopic compositions of both magmatic rocks and regional mineralizations further indicate that the magmatic rocks are seemingly a source of lead for the Nefza ore deposits. Moreover, the emplacement of magmatic rocks has enhanced hydrothermal fluid circulations, leading to the deposition of these mineralizations. All these events occurred during the Late Mio-Pliocene regional extensional context. This predates supergene remobilizations and mineralizations due to weathering, before the occurrence of the last low-temperature hydrothermal event leading to neoformation of polymetallic mineralizations (at least in the whole Oued Belif area).

On the broader scale of the Eastern Maghrebides, the Miocene geodynamic context that led to the emplacement of the Nefza magmatic rocks – namely SCLM source and crustal shear-zone reactivation probably on the former passive margin side (metacraton) – was also conducive to ore deposition. Numerous polymetallic occurrences are indeed present in the area stretching from Nefza to the Cap de Fer (Algeria); that area seems to be the most promising target for the identification of new deposits.

Supplementary data to this article can be found online at http://dx.doi.org/10.1016/j.lithos.2014.02.001.

Acknowledgments

The first author (SD) thanks the Belgian Fund for Scientific Research (FNRS), for providing her with a FRIA PhD grant (years 2004–2008). This research benefits from the 2008–2010 cooperation initiative between Tunisia and Wallonie-Bruxelles International entitled "Valorisation des géomatériaux de la région de Nefza-Sejnane (Nord-Ouest de la Tunisie)" as well as from the 2011–2013 TerMEX project entitled "Systèmes métallogéniques et géodynamique alpine: les minéralisations associées à l'évolution néogène des Maghrébides orientales. Relations avec la tectonique décrochante et le magmatisme post-orogénique". Jacques Navez (Musée royal de l'Afrique centrale) is thanked for its role in providing chemical analyses. The authors would also like to thank Nadine Mattielli and Wendy Debouge from the "Département des Sciences de la Terre et de l'Environnement" (ULB) for preparing samples and acquiring Pb isotopic data and Patricia Hermand (MRAC) for the maintenance of the TIMS. Georges Zaboukis (ULB) is thanked for the confection of thin sections. We thank René Maury and an anonymous reviewer for their incisive comments that contributed to a nice amelioration of this paper.

References

Abdallah, N., Liégeois, J.P., De Waele, B., Fezaa, N., Ouabadi, A., 2007. The Temaguessine Fe-cordierite orbicular granite (Central Hoggar, Algeria): U–Pb SHRIMP age, petrology, origin and geodynamical consequences for the late Pan-African magmatism of the Tuareg shield. J. Afr. Earth Sci. 49, 153–178.

Abidi, R., Slim-Shimi, N., Somarin, A., Henchiri, M., 2010. Mineralogy and fluid inclusions study of carbonate-hosted Mississippi valley-type Ain Allega Pb–Zn–Sr–Ba ore deposit, northern Tunisia. J. Afr. Earth Sci. 57, 262–272.

Abidi, R., Slim-Shimi, N., Hatira, N., Somarin, A., 2011. Genesis of celestite — bearing cap rock formation from the Ain Allega ore deposit (northern Tunisia): contributions from microthermometric studies. Bull. Soc. Geol. Fr. 182, 427–435.

Abidi, R., Slim-Shimi, N., Marignac, C., Hatira, N., Gasquet, D., Renac, C., Soumarin, A., Gleeson, S., 2012. The origin of sulfate mineralization and the nature of the BaSO4–SrSO4 solid-solution series in the Ain Allega and El Aguiba ore deposits, northern Tunisia. Ore Geol. Rev. 48, 165–179.

Aïssa, D.E., Marignac, C., Cheilletz, A., Gasquet, D., 1998. Géologie et métallogénie sommaires du massif bde l'Edough (NE Algérie). Mémoires du Service Géologique de l'Algérie.

Aïssa, D.E., Cheilletz, A., Marignac, C., 2001. Magmatic fluids and skarn mineralization: the Burdigalian As–W skarn at Karézas (Edough Massif, NE Algeria). In: Balkema, A.A. (Ed.), Proceedings of the 6th SGA Meeting, Krakow, Rotterdam, pp. 877–880.

Albidon Limited, 2004. Exploration Report. http://www.albidon.com/documents/Nefza2.pdf.

Azzouni-Sekkal, A., Liégeois, J.-P., Bechiri-Benmerzoug, F., Belaid-Zinet, S., Bonin, B., 2003. The «Taourirt» magmatic province, a marker of the closing stage of the Pan-African orogeny in the Tuareg Shield: review of available data and Sr–Nd isotope evidence. J. Afr. Earth Sci. 56, 107–113.

Badgasarian, G.P., Bajanik, S., Vass, D., 1972. Age radiométrique du volcanisme néogène du Nord de la Tunisie. Notes du Service Géologique de Tunisie. 40, pp. 79–85.

Batik, P., 1980. Carte géologique de la Tunisie; feuille n°11: Hédil. Service Géologique, Office National des Mines (1 sheet).

Belayouni, H., Brunelli, D., Clocchiatti, R., Brunelli, D., Clocchiatti, R., Di Staso, A., Hassani, I.E.E.A.E., Guerrera, F., Kassaa, S., Ouazaa, N.L.M., Manuel, M.M., Serrano, F., Tramontana, M., 2010. La Galite Archipelago (Tunisia, North Africa): stratigraphic and petrographic revision and insights for geodynamic evolution of the Maghrebian Chain. J. Afr. Earth Sci. 56, 15–28.

Bellon, N., 1976. Séries magmatiques néogènes et quaternaires du pourtour de la Méditerranée occidentale comparées dans leur cadre géodynamique. Implications géodynamiques. Unpublished PhD thesis. Université de Paris-Sud/Orsay, 363 p.

Benaouali-Mebarek, N., Frizon de Lamotte, D., Roca, E., Bracene, R., Faure, J.-L., Sassi, W., Roure, F., 2006. Post-Creyaceous kinematics of the Atlas and Tell systems in central Algeria: early foreland folding and subduction-related deformation. C. R. Geosci. 338, 115–125.

Bouabsa, L., Marignac, C., Cuney, M., Gherbi, C., 2005. Le complexe granitique Langhien du Filfila (Nord-Est Constantinois, Algérie): Granites à cordiérite et granites à métaux rares. Nouvelles données minéralogiques et géochimiques et conséquences pétrologiques. Bull. Serv. Géol. Algér. 16–1, 15–53.

Bouaziz, S., Barrier, E., Soussi, M., Turki, M.M., Zouari, H., 2002. Tectonic evolution of the northern African margin in Tunisia from paleostress data and sedimentary record. Tectonophysics 357, 227–253.

Bouillin, J.-P., 1977. Géologie alpine de la Petite Kabylie dans les régions de Collo et d'El-Milia (Algérie). Unpublished Thesis, Pierre and Marie Curie University (Paris 6), 511 p.

Carminati, E., Wortel, M.J.R., Spakman, W., Sabadini, R., 1998. The role of slab detachment processes in the opening of the western–central Mediterranean basins: some geological and geophysical evidence. Earth Planet. Sci. Lett. 160, 651–665.

Coulon, C., Megartsi, M., Fourcade, S., Maury, R.C., Bellon, H., Louni-Hacini, A., Cotten, J., Coutelle, A., Hermitte, D., 2002. Post-collisional transition from calc-alkaline to alkaline volcanism during the Neogene in Oranie (Algeria): magmatic expression of a slab breakoff. Lithos 62, 87–110.

Crampon, N., 1971. Etude géologique de la bordure des Mogods du pays de Bizerte et du Nord des Hédil (Tunisie septentrionale). Unpublished PhD thesis, Nancy 1-University, 522 p.

De Waele, B., Liégeois, J.P., Nemchin, A.A., Tembo, F., 2006. Isotopic and geochemical evidence of Proterozoic episodic crustal reworking within the Irumide belt of South-Central Africa, the southern metacratonic boundary of an Archaean Bangweulu craton. Precambrian Res. 148, 225–256.

Debon, F., Le Fort, P., 1983. A chemical–mineralogical classification of common plutonic rocks and associations. Transactions of the Royal Society of Edinburgh. Earth Environ. Sci 73, 135–149.

Decrée, S., Marignac, C., De Putter, Th., Deloule, E., Liégeois, J.P., Demaiffe, D., 2008a. Pb–Zn mineralization in a Miocene regional extensional context: The case of the Sidi Driss and the Douahria ore deposits (Nefza mining district, northern Tunisia). Ore Geol. Rev. 34, 285–303.

Decrée, S., De Putter, Th., Yans, J., Recourt, Ph., Jamoussi, F., Bruyère, D., Dupuis, Ch., 2008b. Iron mineralization in Pliocene sediments of the Tamra iron mine (Nefza mining district, Tunisia). mixed influence of pedogenesis and hydrothermal alteration. Ore Geol. Rev. 33, 397–410.

Decrée, S., Ruffet, G., De Putter, Th., Baele, J.M., Recourt, Ph., Yans, J., 2010. Mn oxides as efficient traps for metal pollutants in a Fe–Pb–Zn mine environment (Tamra iron mine, Nefza mining district, Tunisia). J. Afr. Earth Sci. 57, 249–261.

Decrée, S., Baele, J.-M., De Putter, Th., Yans, J., Clauer, N., Dermech, M., Aloui, K., Marignac, Ch., 2013. The Oued Belif hematite-rich breccia (Nefza Mining District, NW Tunisia): a potential candidate for a Miocene small-scale iron oxide copper gold (IOCG) deposit in Northern Tunisia. Econ. Geol. 108, 1425–1457.

Dermech, M., 1990. Le complexe de l'Oued Bélif – Sidi Driss (Tunisie septentrionale). Hydrothermalisme et métallogénie. Unpublished PhD thesis, Université de Paris VI, 336p.

Duchesne, J.C., Liégeois, J.P., Vander Auwera, J., Bolle, O., Bruguier, O., Matukov, D.I., Sergeev, S.A., 2013. The fast evolution of a crustal hot zone at the end of a transpressional regime: the Saint-Tropez peninsula granites and related dykes (Maures Massif, SE France). Lithos 162–163, 195–220.

Ennih, N., Liégeois, J.P., 2008. The boundaries of the West African craton, with a special reference to the basement of the Moroccan metacratonic Anti-Atlas belt. In: Ennih, N., Liégeois, J.P. (Eds.), Thec Boundaries of the West African Craton. Geological Society, London, Special Publications, 297, pp. 1–17.

Faul, H., Foland, K., 1980. L'âge des rhyodacites de Nefza-Sedjenane. Notes du Service Géologique de Tunisie n°46. Trav. Géol. Tunis. 14, 47–49.

Fourcade, S., Capdevila, R., Ouabadi, A., Martineau, F., 2001. The origin and geodynamic significance of the Alpine cordierite-bearing granitoids of northern Algeria. A combined petrological, mineralogical, geochemical and isotopic O, H, Sr, Nd/study. Lithos 57, 187–216.

Frizon de Lamotte, D., Saint-Bezar, B., Bracene, R., Mercier, E., 2000. The two main steps of the Atlas building and geodynamics of the western Mediterranean. Tectonics 19, 740–761.

Frizon de Lamotte, D., Michard, A., Saddiqi, O., 2006. Quelques développements récents sur la géodynamique du Maghreb. Compt. Rendus Geosci. 338, 1–10.

Gelabert, B., Sabat, F., Rodriguez-Perea, A., 2002. A new proposal for the late Cenozoic geodynamic evolution of the western Mediterranean. Terra Nova 14, 93–100.

Gharbi, M., 1977, Etude des minéralisations mercurifères de l'accident Ghardimaou-Cap Serrat (Tunisie du Nord-Ouest): Unpublished MSc thesis, Ecole Nationale Supérieure de Géologie Appliquée et de Prospection Minière de Nancy, 131 p.

Gottis, Ch., Sainfeld, P., 1952. Les gîtes métallifères tunisiens: XIXème Congrès Géologique International. Monographies régionales, 2e série, Tunisie. no 2 (104 pp.).

Gueguen, E., Doglioni, C., Fernandez, M., 1998. On the post-25 Ma geodynamic evolution of the western Mediterranean. Tectonophysics 298, 259–269.

Guerrera, F., Martin-Algarra, A., Perrone, V., 1993. Late Oligocene–Miocene syn-late-orogenic successions in Western and Central Mediterranean Chains from the Betic Cordillera to the Southern Apennines. Terra Nova 5, 525–544.

Hadj, Kaddour Z., Liégeois, J.P., Demaiffe, D., Caby, R., 1998. The alkaline–peralkaline granitic post-collisional Tin Zebane dyke swarm (Pan-African Tuareg shield, Algeria): prevalent mantle signature and late agpaitic differentiation. Lithos 45, 223–243.

Halloul, N., 1989. Géologie, pétrologie et géochimie du bimagmatisme néogène de la Tunisie septentrionale (Nefza et Mogod). Implications pétrogénétiques et interprétation géodynamique. Unpublished thesis, Université Baise Pascal, Clermont Ferrand.

Halloul, N., Gourgaud, A., 2012. The post-collisional volcanism of northern Tunisia: petrology and evolution through time. J. Afr. Earth Sci. 63, 62–76.

Handy, M.R., Schmid, S.M., Bousquet, R., Kissling, E., Bernouilli, D., 2010. Reconciling plate-tectonic reconstructions of Alpine Tethys with the geological–geophysical records of spreading and subduction in the Alps. Earth Sci. Rev. 102, 121–158.

Hernandez, J., de Larouzière, F.D., Bolze, J., Bordet, P., 1987. Le magmatisme néogene bético-rifain et le couloir de decrochement trans-Alboran. Bull. Soc. c de France v. III 257–267.

Jallouli, C., Mickus, K., 2000. Regional gravity analysis of the crustal structure of Tunisia. J. Afr. Earth Sci. 30, 53–78.

Jallouli, C., Inoubli, M.H., Alboui, Y., 1996. Le corps igné de Nefza (Tunisie septentrionale): caractéristiques géophysiques et discussion du mécanisme de sa mise en place. Notes Serv. Géol. Tunisie 109–123.

Jallouli, C., Mickus, K., Turki, M.M., Rihane, C., 2003. Gravity and aeromagnetic constraints on the extent of Cenozoic rocks within the Nefza–Tabarka region, northwestern Tunisia. J. Volcanol. Geotherm. Res. 122, 51–68.
Jolivet, L., 2008. Géodynamique méditerranéenne. In: Jolivet, L., et al. (Eds.), Géodynamique méditerranéenne. Société Géologique de France, Vuibert, pp. 5–47.
Juteau, M., Michard, A., Albarede, F., 1986. The Pb–Sr–Nd isotope geochemistry of some recent circum-Mediterranean granites. Contrib. Mineralogy Petrol. 92, 331–340.
Krauskopf, K.B., 1970. Tungsten. In: Wedepohl, H.K. (Ed.), Handbook of Geochemistry. vol. 5. Springer, New York.
Laridhi Ouazaa, N., 1988. Premières descriptions pétrographiques de la série de pyroclastites du bassin sédimentaire mio-pliocène de l'oued Zouara (Nefza, Tunisie septentrionale). C. R. Acad. Sci. 307, 2055–2060.
Laridhi Ouazaa, N., 1989a. Principales caractéristiques géochimiques des laves basiques miocènes de la Tunisie septentrionale: Nefza et Mogod. C. R. Acad. Sci. Séries IIA 308, 1055–1060.
Laridhi Ouazaa, N., 1989b. Mise en évidence dune identité minéralogique et géochimique entre la rhyodacite de Ain Deflaia et les pyroclastites du bassin sédimentaire de Oued Zouara (Nefza: Tunisie septentrionale). C. R. Acad. Sci. Séries IIA 309, 1571–1576.
Laridhi Ouazaa, N., 1990. Etude minéralogique des laves basiques miocènes de la Tunisie Septentrionale (Nefza et Mogod). C. R. Acad. Sci. Séries IIA 311, 1207–1212.
Laridhi Ouazaa, N., 1996. Etude minéralogique et géologique des épisodes magmatiques mésozoïques et miocènes de la Tunisie. Unpublished PhD thesis, Université de Tunis II, 466 p.
Le Maitre, R.W., Streckeisen, A., Zanettin, B., Le Bas, M.J., Bonin, B., Bateman, P., Bellieni, G., Dudek, A., Efremova, S., Keller, J., Lameyre, J., Sabine, P.A., Scmid, R., Sorensen, H., Woolley, A.R., 2002. Igneous Rocks: A Classification and Glossary of Terms: Recommendations of the International Union of Geological Sciences, Subcommission on the Systematics of Igneous Rocks. Cambridge University Press (236 pp.).
Liégeois, J.-P., Navez, J., Hertogen, J., Black, R., 1998. Contrasting origin of post-collisional high-K calc-alkaline and shoshonitic versus alkaline and peralkaline granitoids. The use of sliding normalization. Lithos 45, 1–28.
Liégeois, J.P., Latouche, L., Boughrara, M., Navez, J., Guiraud, M., 2003. The LATEA metacraton (Central Hoggar, Tuareg shield, Algeria): behaviour of an old passive margin during the Pan-African orogeny. J. Afr. Earth Sci. 37, 161–190.
Liégeois, J.P., Benhallou, A., Azzouni-Sekkal, A., Yahiaoui, R., Bonin, B., 2005. The Hoggar swell and volcanism: reactivation of the Precambrian Tuareg shield during Alpine convergence and West African Cenozoic volcanism. In: Foulger, G.R., Natland, J.H., Presnall, D.C., Anderson, D.L. (Eds.), Plates, plumes. Series 'special paper'. Boulder. Geological Society of America, 388, pp. 379–400.
Liégeois, J.P., Abdelsalam, M.G., Ennih, N., Ouabadi, A., 2013. Metacraton: nature, genesis and behavior. Gondwana Res. 23, 220–237.
Ludwig, K.R., 2003. Isoplot 3.00, a geochronological toolkit for Microsoft Excel. Berkeley Geochronology Center Special Publication. n°4 (69 pp.).
Lugmair, G.W., Marti, K., 1978. Lunar initial 143Nd/144Nd: differential evolution of the lunar crust and mantle. Earth Planet. Sci. Lett. 39, 349–357.
Lustrino, M., Wilson, M., 2007. The circum-Mediterranean anorogenic Cenozoic igneous province. Earth Sci. Rev. 81, 1–65.
Marignac, C., 1985. Les minéralisations filoniennes d'Aïn Barbar (Algérie): un exemple d'hydrothermalisme lié à l'activité géothermique alpine en Afrique du Nord. Unpublished Doctorat d'Etat Thesis, INPL, Nancy, 2 vol., 1163 p.
Marignac, C., 1988a. A case of ore deposition associated with geothermal activity: the polymetallic ore veins of Aïn Barbar (NE Constantinois, Algeria). Mineral. Petrol. 39, 107–127.
Marignac, C., 1988b. P–T–X evolution of ore veins associated with paleogeothermal activity: the polymetallic ore veins of Aïn Barbar (NE Constantinois, Algeria): reconstruction from fluid inclusion data. Bull. Mineral. 111, 359–381.
Mascle, G.H., Tricart, P., Torelli, L., Bouillin, J.P., Compagnoni, R., Depardon, S., Mascle, J., Pecher, A., Peis, D., Rekhiss, F., Rolfo, F., Bellon, H., Brocard, G., Lapierre, H., Monié, P., Poupeau, G., 2004. Structure of the Sardinia Channel: crustal thinning and tardi-orogenic extension in the Apenninic–Maghrebian orogen; results of the Cyana submersible survey (SARCYA and SARTUCYA) in the western Mediterranean. Bull. Soc. Geol. Fr. 175, 607–626.
Mauduit, F., 1978. Le volcanisme néogène de la Tunisie continentale. Unpublished thesis, Université de Paris Sud. 157 p
Maury, R.C., Fourcade, S., Coulon, C., El Azzouzi, M., Bellon, H., Coutelle, A., Ouabadi, A., Semroud, B., Megartsi, M., Cotten, J., Belanteur, O., Louni-Hacini, A., Piqué, A., Capdevila, R., Hernandez, J., Réhault, J.-P., 2000. Post-collisional Neogene magmatism of the Mediterranean Maghreb margin: a consequence of slab breakoff. C. R. Acad. Sci. 331, 159–173.
McDonough, W.F., 1990. Constraints on the composition of the continental lithospheric mantle. Earth Planet. Sci. Lett. 101, 1–18.
Metrich-Travers, N., 1976. Fusion partielle dans les enclaves gneissiques. Applications aux volcanismes de Toscane et de Tunisie. Unpublished thesis, Orsay-France, 170 p.
Michard, A., Negro, F., Saddiqi, O., Bouybaouene, M.L., Chalouan, A., Montigny, R., Goffé, B., 2006. Pressure–temperature–time constraints on the Maghrebide mountain building: evidence from the Rif–Betic transect (Morroco, Spain), Algerian correlations, and geodynamic implications. Compt. Rendus Geosci. 338, 92–114.
Missenard, Y., Cadoux, A., 2012. Can Moroccan Atlas lithospheric thinning and volcanism be induced by Edge-Driven Convection? Terra Nova 24, 27–33.
Moussi, B., Medhioub, M., Hatira, N., Yans, J., Hajjaji, W., Rocha, F., Labrincha, J.A., Jamoussi, F., 2011. Identification and use of white clayey deposits from the area of Tamra (northern Tunisia) as ceramic raw materials. Clay Miner. 46, 165–175.
Negra L., 1987. Pétrologie, minéralogie et géochimie des minéralisations et des roches encaissantes des basins associés aux structures tectoniques et magmatiques de l'Oued Bélif et du Jebel Haddada (Nord des Nefza, Tunisie septentrionale). Unpublishe PhD thesis, Université de Paris-Sud, 223p.
Nkono, C., Femenias, O., Diot, H., Berza, T., Demaiffe, D., 2006. Flowage differentiation in an andesitic dyke of the Motru Dyke Swarm (Southern Carpathians, Romania) inferred from AMS, CSD and geochemistry. J. Volcanol. Geotherm. Res. 154, 201–221.
Perthuisot, V., 1978. Dynamique et pétrogenèse des extrusions triasiques de Tunisie septentrionale: Travaux du Laboratoire de Géologie. Presse de l'Ecole Normale Supérieure de Paris. v. 12 (312 pp.).
Piqué, A., Ait Brahim, L., El Azzouzi, M.H., Maury, R., Bellon, H., Semroud, B., Laville, E., 1998. Le poinçon maghrébin: contraintes structurales et géochimiques. C. R. Acad. Sci. Paris 326, 575–581.
Piqué, A., Tricart, P., Guiraud, R., Laville, E., Bouaziz, S., Amrhar, M., Ait Ouali, R., 2002. The Mesozoic–Cenozoic Atlas belt (North Africa): an overview. Geodin. Acta 15, 185–208.
Rekhiss, F., 2007. Modèle d'évolution structural et géodynamique à l'extrémité orientale de la chaine alpine d'Afrique du Nord. Unpublished PhD thesis. El-Manar University, Tunis, 285p.
Rhoden, H.N., Ereño, I., 1961. Magnetite ores of Northern Morocco. Trans. Inst. Min. Metall. 71, 629–661.
Rouvier, H., 1977. Géologie de l'extrême Nord-Tunisien: tectoniques et paléogéographie superposées à l'extrémité orientale de la chaîne Nord-Maghrebine. Unpublished PhD thesis. Université Pierre et Marie Curie, Paris, France, 215p.
Rouvier, H., 1987. Carte Géologique de la Tunisie, feuille n°10 (Nefza — 1/50,000). Tunisian Office for Topography and Cartography (1 sheet).
Shang, C.K., Satir, M., Nsifa, E.N., Liegeois, J.P., Siebel, W., Taubald, H., 2007. Archaean high-K granitoids produced by remelting of earlier Tonalite–Trondhjemite–Granodiorite (TTG) in the Sangmelima region of the Ntem complex of the Congo craton, southern Cameroon. Int. J. Earth Sci. 96, 817–841.
Shang, C.K., Liégeois, J.P., Satir, M., Frisch, W., Nsifa, E.N., 2010. Late Archaean high-K granite geochronology of the northern metacratonic margin of the Archaean Congo craton, southern Cameroon: Evidence for Pb-loss due to non-metamorphic causes. Gondwana Res. 18, 337–355.
Slim-Shimi, N., Moëlo, Y., Tlig, S., 1990. Caractérisation minéralogique et signifiance métallogénique des sulfures bismuthifères des minéralisations de La Galite et du Jebel Chouichia (NW de la Tunisie). C. R. Acad. Sci. 311, 127–132.
Steiger, R.H., Jäger, E., 1977. Subcommission on geochronology: convention on the use of decay constants in geo- and cosmochronology. Earth Planet. Sci. Lett. 36, 359–362.
Stussi, J.-M., Cuney, M., 1993. Modèles d'évolution géochimique de granitoïdes peralumineux. L'exemple du complexe plutonique varisque du Millevaches (Massif Central français). Bull. Soc. Geol. Fr. 164, 585–596.
Sun, S.S., 1982. Chemical composition and origin of the Earth's primitive mantle. Geochim. Cosmochim. Acta 46, 179–192.
Sun, S.S., McDonough, W.F., 1989. Chemical and isotopic systematics of oceanic basalts: implications for Mantle composition and processes. Geol. Soc. Lond., Spec. Publ. 42, 313–345.
Talbi, F., Slim-Shimi, N., Tlig, S., Zargouni, F., 1999. Nature, origine et évolution des fluides dans le district minier de la caldeira d'Oued Bélif (Nefza, Tunisie septentrionale). C. R. Acad. Sci. 328, 153–160.
Talbi, F., Jaafari, M., Tlig, S., 2005. Magmatisme néogène de la Tunisie septentrionale: pétrogénèse et événements géodynamiques. Rev. Soc. Geol. Esp. 18, 241–252.
Toummite, A., Liégeois, J.P., Gasquet, D., Bruguier, O., Beraaouz, E.H., Ikenne, M., 2013. Field, geochemistry and Sr–Nd isotopes of the Pan-African granitoids from the Tifnoute Valley (Sirwa, Anti-Atlas, Morocco): a post-collisional event in a metacratonic setting. Mineral. Petrol. 107, 739–763.
Tricart, P., Torelli, L., Argnani, A., Rekhiss, F., Zitellini, N., 1994. Extensional collapse related to compressional uplift in the Alpine Chain off northern Tunisia (Central Mediterranean). Tectonophysics 238, 317–329.
Tzekova, V., 1975. Zone du volcanisme Tabarka-Sedjenane. Région d'Oued Bélif. Rapport géologique au 1/5000e et prospection. Phasa IV. TECHNOEXPORTSTROY-BULGARPROREMI, Bulgarie, Rapport non publié, Office National des Mines.
Weis, D., Kieffer, B., Maerschalk, C., Barling, J., De Jong, J., Williams, G., Hanano, D., Pretorius, W., Mattielli, N., Scoates, J.S., Goolaerts, A., Friedman, R., Mahoney, J.B., 2006. High-precision isotopic characterization of USGS reference materials by TIMS and MC-ICP-MS. Geochem. Geophys. Geosyst. 7. http://dx.doi.org/10.1029/2006GC001283.
Yelles-Chaouche, A., Boudiaf, A., Djellit, H., Bracene, R., 2006. La tectonique active de la région nord-algérienne. C. R. Géosci., 338, pp. 126–139.
Zartman, R.E., Doe, B.R., 1981. Plumbotectonics — the model. Tectonophysics 75, 135–162.
Zartman, R.E., Haines, S.M., 1988. The plumbotectonic model for Pb isotopic systematics among major terrestrial reservoirs) a case for bi-directional transport. Geochim. Cosmochim. Acta 52, 1327–1339.
Zouiten, S., 1999, Application de la géothermométrie chimique aux eaux des sources thermales du Nord de la Tunisie: Unpublished PhD Thesis, Tunis II University, Tunis, 197 p.